ADVANCING EARTH AND SPACE SCIENCE

JGR Atmospheres

RESEARCH ARTICLE
10.1029/2020JD034219

Revisiting the Surface Energy Imbalance

Jielun Sun[1], William J. Massman[2], Robert M. Banta[3,4], and Sean P. Burns[5,6]

[1]NorthWest Research Associates, Boulder, CO, USA, [2]USDA/Forest Service, Rocky Mountain Research Station, Fort Collins, CO, USA, [3]CIRES, University of Colorado, Boulder, CO, USA, [4]NOAA/Earth System Research Laboratory/Chemical Sciences Laboratory, Boulder, CO, USA, [5]National Center for Atmospheric Research, Boulder, CO, USA, [6]Department of Geography, University of Colorado, Boulder, CO, USA

Key Points:

- The surface energy balance is found to be related to both thermal and kinetic energy balances based on total energy conservation
- Energy transfers missed in the traditional imbalance studies are identified in the interfaced soil and the atmospheric layers
- The imbalance is highly related to energy dissipation as a result of non-hydrostatic energy transfer in the stratified atmosphere

Correspondence to:
J. Sun,
jielun@nwra.com

Citation:
Sun, J., Massman, W. J., Banta, R. M., & Burns, S. P. (2021). Revisiting the surface energy imbalance. *Journal of Geophysical Research: Atmospheres*, *126*, e2020JD034219. https://doi.org/10.1029/2020JD034219

Received 11 NOV 2020
Accepted 16 MAY 2021

Author Contributions:
Conceptualization: Jielun Sun
Data curation: Jielun Sun
Formal analysis: Jielun Sun
Investigation: Jielun Sun
Methodology: Jielun Sun
Resources: Jielun Sun, William J. Massman, Robert M. Banta, Sean P. Burns
Software: Jielun Sun
Supervision: Jielun Sun
Validation: Jielun Sun
Visualization: Jielun Sun
Writing – original draft: Jielun Sun
Writing – review & editing: Jielun Sun, William J. Massman, Robert M. Banta, Sean P. Burns

Abstract The traditional surface energy balance (SEB) is investigated by applying the thermal energy balance based on total energy conservation. Based on total energy conservation, the thermal and the kinetic energy balances are connected through non-hydrostatic energy transfer (Q_{NH}) as a result of the hydrostatic imbalance caused by potential energy changes from vertical density fluxes in response to mechanical and thermal forcing in the stratified atmosphere. Field observations show that both Q_{NH} and the surface energy imbalance (SEI) have the same diurnal variation; both are near zero under neutral conditions and increase with increasing atmospheric unstable stratification. Energy dissipation due to enhanced turbulent kinetic energy from Q_{NH} is estimated to be the largest energy consumption for potentially explaining the largest SEI under free convective conditions. The relatively large value of energy dissipation in the atmospheric surface layer is due to its exponential increase toward the surface and its increase with atmospheric instability. The other two energy transfers that are traditionally missed are related to water mass flowing through the open soil and air layers, but are relatively small in comparison with the energy dissipation. The new understanding of the energy transfers provides not only a potential explanation for the temporal and magnitude variations of the SEI but also the explanation for different heat/moisture transferring efficiencies between thermally and mechanically generated turbulent mixing. Understanding the SEB is important not only for solving the SEI but also for understanding energy conservation in the atmosphere.

1. Introduction

The concept of equal upward and downward thermal energy fluxes across the earth surface is the key argument behind the traditional surface energy balance (SEB) "since the earth's surface is a boundary interface and can absorb no energy" as Geiger et al. (1995) (first edition: Geiger, 1927) described it. The earliest discussion on the SEB that we can find is by Albrecht (1937, 1940). Being able to observe the SEB with all measured energy transfers is critically important to ensure our understanding of energy transfers in the atmospheric thermodynamics.

The traditional SEB over flat terrain without vegetation is commonly expressed as the balance among the net radiation at the surface, R_{net}, the sensible heat flux, Q_H and the latent heat flux, Q_E at a given height z, and the downward soil heat flux at the surface, Q_{Gsfc}, which is also called the ground heat flux (Foken, 2017), that is,

$$R_{net} = Q_H + Q_E + Q_{Gsfc}, \tag{1}$$

where

$$Q_{Gsfc} = Q_G + \Delta Q_S. \tag{2}$$

In the literature, Q_{Gsfc} is often considered as the downward soil heat flux corrected to the soil surface. That is, Q_{Gsfc} is derived with the commonly observed downward soil heat flux measured at a distance below the surface, Q_G, and inclusion of the soil heat storage between the depth where Q_G is measured and the surface due to soil temperature changes, ΔQ_S (e.g., Kustas & Daughtry, 1990; Li & Wang, 2020; Liebethal & Foken, 2007; Liebethal et al., 2005). However, most of the sites in the global FLUXNET tower network do not report ΔQ_S (e.g., Stoy et al., 2013). Any observed surface energy imbalance (SEI) from Equation 1 is expressed as the residual of the SEB, Q_{res}, as

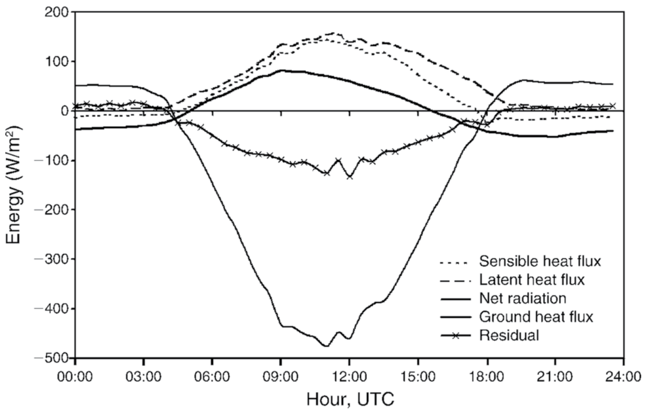

Figure 1. Adapted from Figure 4, Foken (2008). Note that the negative surface energy imbalance (residual) here corresponds to the positive turbulent energy transfers plotted here.

$$Q_{res} = R_{net} - Q_{Gsfc} - Q_H - Q_E. \tag{3}$$

That is, the residual of the SEI, by definition, is positively related to the available energy $R_{net} - Q_{Gsfc}$ and negatively related to turbulent energy transfers, Q_H and Q_E. Often, the ratio r between the turbulent thermal energy transfer $Q_H + Q_E$ and the available energy $R_{net} - Q_{Gsfc}$,

$$r = \frac{Q_H + Q_E}{R_{net} - Q_{Gsfc}}, \tag{4}$$

is used as a measure of the SEI if r deviates from unity. Evidently, r may be ill-defined, when $|R_{net} - Q_{Gsfc}|$ approaches zero, leading to large uncertainty in quantifying the magnitude of the imbalance.

Results from numerous field-measurement studies have shown a consistent and systematic inability to balance the SEB (e.g., Aubinet et al., 1999; Foken, 2008; Foken et al., 2010, 2011; Leuning et al., 2012; Oncley et al., 2007; Twine et al., 2000; Wilson et al., 2002). As illustrated in Figure 1, this observed SEI, on average, varies diurnally—the available energy is larger than the sum of the turbulent energy transfers during daytime ($Q_{res} > 0$) with the largest Q_{res} around noon, less than the sum at night ($Q_{res} < 0$) with a relatively small value of Q_{res}, and is equal to the sum around the morning and the evening transition periods ($|Q_{res}| \approx 0$) (e.g., Foken, 2008; Oncley et al., 2007; Panin & Bernhofer, 2008). Although the magnitude of the SEI is largest during daytime, but when considered as a fraction of percentage deviation, r is greater at night (e.g., Kidston et al., 2010; Wilson et al., 2002).

Understanding the SEB relies on the thermal energy balance. Guided by total energy conservation, Sun (2019) found that the fact of turbulence kinetic energy (TKE) changes through thermal energy transfer, such as surface heating to thermal plumes, is recognized in the kinetic energy balance but ignored in the thermal energy equation. In the stratified atmosphere, this energy transfer is important (more later). The systematic SEI and the recent energy conservation study prompt us to re-examine the SEI. In this study, we mainly explore the effects of including the missed energy transfer in the thermal energy equation in the SEI and how its inclusion may explain the SEI. We also investigate efficiency effects of turbulent heat and moisture transfers near the surface, where the major thermal energy source/sink for the atmospheric stratification is located. We first briefly describe traditional investigations of the SEB in the literature, and discuss key physical concepts relevant to the SEI but not clearly addressed yet in the literature (Section 2). We then examine the thermal energy balance in the air layer above the surface and the soil layer that interfaces with the air layer by focusing on the key physical processes that are missed in the traditional SEB study (Section 3). Based on field observations described in Section 4, we estimate all the energy transfers that contribute to the SEI with special focus on physical processes when the largest SEI is observed under free convective conditions in Section 5. The important conclusions are summarized in Section 6.

2. A Brief Review of the Surface Energy Imbalance

2.1. Historical Investigations

The SEB has been used to judge the eddy correlation method for obtaining Q_H and Q_E soon after the technique was invented (e.g., Elagina et al., 1973; Foken & Oncley, 1995; Kaimal, 1978; Suomi, 1957; Swinbank, 1951). Numerous studies on the SEI have been published since its first formulation more than 80 years ago, and are reviewed by many authors (e.g., Foken et al., 2011; Leuning et al., 2012; Mauder et al., 2020). Here we only briefly summarize some major hypotheses for the SEI with a few references given the massive amount of the SEB work in the literature. Most of the investigations of the SEI focus on measurement issues in the atmosphere such as mismatch of footprints for the measured energy transfer terms in the SEB (e.g., Finnigan, 2004a), measurement errors due to phase differences between variables and instrument misalignments (e.g., Horst & Lenschow, 2009), wind speed correction for sonic anemometers (Burns et al., 2012; Horst et al., 2015), sonic-anemometer structural issues (e.g., Frank et al., 2016; Nakai et al., 2014), unaccounted horizontal energy transports (e.g., Aubinet et al., 2003; Culf et al., 2004; Mahrt et al., 1994, 2001; Sun et al., 1997; Oliphant et al., 2004; Sun et al., 2007; Sun & Mahrt, 1994), non-stationarity of turbulent mixing (e.g., Mahrt, 1998), turbulence averaging time (e.g., Finnigan et al., 2003; Mauder & Foken, 2006), estimation of soil heat storage (e.g., Heusinkveld et al., 2004; Jacobs et al., 2008) and canopy heat storage (e.g., Haverd et al., 2007; Lindroth et al., 2010), and unaccounted energy transfers associated with large-scale eddies or secondary circulations due to insufficient averaging time, especially over heterogeneous surfaces (e.g., Brötz et al., 2014; Charuchittipan et al., 2014; Finnigan, 2004b; Finnigan et al., 2003; Mauder & Foken, 2006; Roo & Mauder, 2018).

With careful estimates of instrument errors, Oncley et al. (2007) found that the imbalance exceeds the estimated measurement errors. Charuchittipan et al. (2014) explored the extension of the averaging time for obtaining sensible and latent heat fluxes used in the SEB, and concluded that increasing averaging time cannot solve the SEI problem in general. Oliphant et al. (2004) found that footprint mismatches do not significantly impact the imbalance. Oliphant et al. (2004) and Leuning et al. (2012) concluded that heat advection cannot explain the SEI in general. Other factors that could affect turbulent mixing and potentially contribute to the SEI such as soil moisture (e.g., Burns et al., 2015; Mauder et al., 2007), friction velocity (e.g., Barr et al., 2006; Oliphant et al., 2004; Sánchez et al., 2010; Wilson et al., 2002), and canopy heat storage and biological processes (e.g., Jacobs et al., 2008; Oke, 2002; Oliphant et al., 2004; Oncley et al., 2007; Wilson et al., 2002) have also been explored. Available studies to date have failed to eliminate the systematic SEB residual in general but only reduce it at some sites; thus, the systematic imbalance still exists for majority of balance investigations.

Currently, the major focus of addressing the SEI seems to be on unstable conditions associated with buoyancy-driven large local circulations resulting from landscape heterogeneity that cannot be captured at a fixed location (e.g., Foken, 2008; Mauder et al., 2010, 2020; Panin & Bernhofer, 2008; Stoy et al., 2013). Although Eder et al. (2015) found that local circulations could extend to the surface, Steinfeld et al. (2007) concluded that organized turbulence structures cannot explain the observed imbalance due to their small magnitudes near the surface in transporting thermal energy. Relevant to this discussion, Sun et al. (2016) found that the strongest vertical energy-transferring turbulence eddies (those with the largest vertical velocity variance [Lenschow & Sun, 2007]) at an observation height z over a homogeneous surface scale with z under both strong-wind and convective conditions. This result implies that when mesoscale circulations approach the surface, the local wind speed at z is enhanced such that the enhanced bulk wind shear at z relative to the surface would generate the strongest energy transferring eddies at the scale of z. Even though mesoscale circulations with scale larger than z can be important in transporting energy far above z (e.g., Sun et al., 1996), on average, their direct contribution to vertical energy transfer at z is relatively small near the surface in comparison with the most energetic turbulence eddies with scale z. This result suggests that vertical energy transfer by mesoscale circulations themselves is important in transferring energy in the atmospheric boundary layer but is unlikely to be important very close to the surface as the ultimate explanation for the SEI in general.

Overall, the above mentioned explanations may reduce the SEI at some sites, but none can explain the systematic diurnal variation of the imbalance over a variety of surfaces. Consequently the observed SEI often results in a lack of confidence in turbulent flux measurements using the eddy-correlation measurement technique to the extent that enhancing observed turbulent fluxes from eddy correlation measurements by an adjustment factor has been a proposed remedy (Huang et al., 2008; Kanda et al., 2004; Panin & Bernhofer, 2008; Twine et al., 2000). The observed systematic SBI is commonly ignored in numerical models.

2.2. Important Concepts Relevant to the SEB

The traditional SEB concept emphasizes the energy balance at the air-surface interface, whereas the concept of energy conservation should be applied to a finite volume of mass such as to a soil layer below the surface with a finite depth. Even with a proper formulation of the SEB for a finite layer, several important physical processes have been overlooked in investigations of the SEI.

First, Geiger et al (1995) (p. 34) described the physical processes at the air-soil interface clearly, stating:

> "Study of fluid flow also shows that in places where the air comes into contact with a solid surface such as the ground or a wall, turbulence and hence eddy diffusion do not extend to the solid. A layer of air a few millimeters thick adheres with great tenacity to the wall or the ground. This is termed the laminar boundary layer. The laws of eddy diffusion are not valid in this layer, but transition from the solid surface to turbulent air is completed within it, governed only by the laws of molecular physics. In this layer, heat is transported only by conduction, and water vapor and other atmospheric elements only by diffusion. This laminar boundary layer constitutes a formidable barrier to the transfer of energy, mass and momentum ..."

That is, any material and energy exchange between Earth and the atmosphere is through molecular thermal conduction or molecular diffusion (e.g., De Groot & Mazur, 2013). Molecular diffusion for heat transfer, which depends on temperature differences across the air-land interface, is a much slower physical process compared to turbulent mixing in the atmosphere, and is confined in a thin air layer adjacent to the surface where turbulent mixing is not effective (Foken, 1978). Therefore, molecular diffusion and its distinctive characteristics in transferring thermal energy are important but overlooked in studying the SEB. The key issue in the SEB is whether we can obtain molecular diffusion of heat transfer across the surface by measuring all the other heat transfers in the thermal energy balance of the air layer below the turbulence measurement height assuming the energy transfers in the soil layer can be properly measured.

Second, Sun (2019) recently found that the traditional thermal energy balance is based on the first law of thermodynamics, which is only valid for flow at rest with zero kinetic energy as described in Batchelor (1967). Because the air motion within a soil layer is negligibly small, the traditional thermal energy balance based on the first law of thermodynamics traditionally used in meteorology is valid for the soil layer. For the dynamic atmosphere, where air motion is strongly influenced by diabatic or non-adiabatic net heating Q and mechanical work $\left[-\nabla \cdot \left(p\mathbf{V}\right) + \epsilon\right]$, where ϵ, p, and $\mathbf{V}$ are viscous stress, pressure, and the wind vector, respectively, the thermal energy balance should be constrained by total energy conservation as practiced in engineering. Total energy conservation has also been referred to as the first law of thermodynamics (e.g., Bennett & Myers, 1962; Bird et al., 2007; Kuo, 2005). Based on total energy conservation for the atmosphere, the sum of kinetic, thermal, and potential energy changes is balanced by $[Q-\nabla\cdot(p\mathbf{V}) + \epsilon]$ (Appendix A). For the atmosphere, surface heating/cooling provides thermal energy to the atmosphere through molecular movement in the molecular diffusion layer while turbulent mixing above consists of organized observable air motions beyond random molecule movements and is characterized with kinetic energy. Thermal expansion/compression as a result of thermal diffusion at the surface would lead to air density changes when turbulent mixing is not effective in transferring heat, leading to vertical variations of air density. When air density increases with height such as during daytime, positive buoyancy generates turbulent mixing, resulting in negative vertical density fluxes. When air density decreases with height such as at night, shear-generated turbulent mixing results in positive vertical density fluxes. In either situation, the vertical density flux results in atmospheric potential energy changes, which disturbs the background hydrostatic balance. The hydrostatic imbalance would generate non-hydrostatic energy transfer in changing TKE based on kinetic energy conservation. Thus, the surface thermal energy transfer actually provides energy not only to thermal energy changes in the atmosphere but also to kinetic energy changes as evident in development of thermal plumes. Constrained by total energy conservation, if the potential energy change leads to a TKE increase, the same amount of energy has to be reduced in the thermal energy balance. Without properly counting for all the energy transfers in the traditional thermal energy balance, which is the key energy balance used in investigating the SEB, the SEI needs to be revisited in light of total energy conservation. A brief demonstration of derivation of the new thermal energy balance from an angle slightly different from Sun (2019) is given in Appendix A and schematically illustrated in Figure 2.

Third, either a soil or an air layer is an open system (e.g., Bird et al., 2007). As a water flow, either liquid or vapor, goes through an open system, the thermal energy of the system may vary when the temperature of the water flow into and out of the system changes even though the water mass within the system remains the same. Hillel (1980) (P. 300) stated that "Temperature gradients affect the moisture potential field and induce both liquid and vapor movement. Reciprocally moisture gradients move water which carries heat." Water movement in soil can be driven by capillary water flow induced by soil water gradients as a result of soil

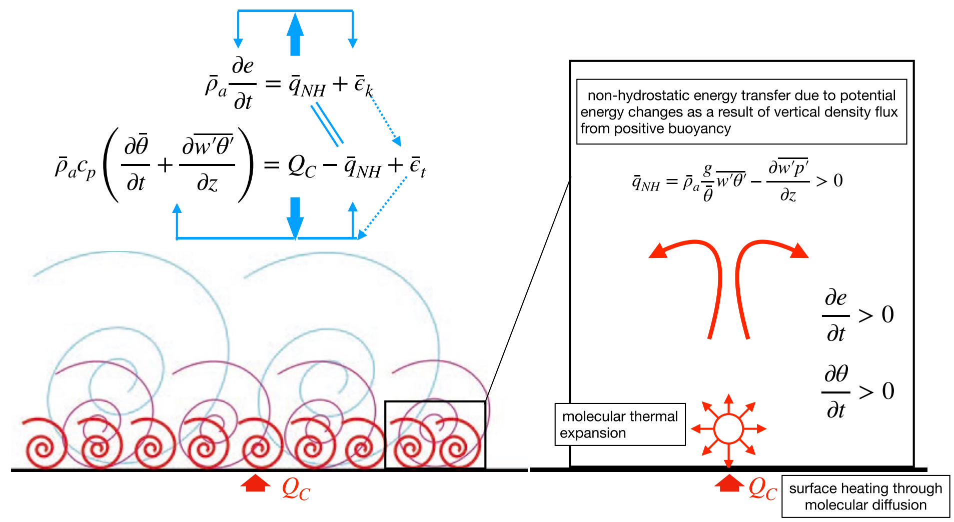

Figure 2. Illustration of energy transfers (following the blue arrows) from the surface heating Q_C to kinetic and thermal energy increases with zero mean wind ($E_m = 0$) and negligible radiative heating in the air layer. As the air at the surface is heated by molecular diffusion Q_C, air expansion leads to the air density decrease adjacent to the surface (right panel). The resulting positive buoyancy, that is, the negative air density flux, disturbs the background hydrostatic balance; hydrostatic imbalance generates a positive non-hydrostatic energy transfer, $\overline{q}_{NH}$, which decreases potential energy of the air layer. Based on kinetic energy conservation, $\overline{q}_{NH}$ enhances turbulence kinetic energy (TKE), e, as evident in thermal plume development (bottom left), which, in turn, enhances TKE dissipation $\overline{\epsilon}_k$ and dissipation heat $\overline{\epsilon}_t$. The energy transfer process under convective conditions prevents Q_C from being effectively transferred upward such that the heat flux at z, $\overline{w'\theta'}$ is not equal to Q_C. Physically, Q_C occurs in the molecular diffusion layer (MDL) adjacent to the surface, and the kinetic and the thermal energy balances here are for the energy transfers in the turbulence surface layer (TSL) above the MDL, where the MDL and the TSL are illustrated in Figure 3. We include Q_C here to illustrate the energy source for all the energy transfers in the TSL under free convective conditions.

evaporation, either in air pockets or at the Earth surface (Heitman et al., 2008; Yamanaka & Yonetani, 1999) and water vapor transport from the surface to the atmospheric boundary layer. As the consequence of the diurnal variations of the surface temperature due to solar heating during daytime and longwave cooling at night, temperature in both the soil and air layers joint at the surface varies vertically. The thermal energy change associated with water mass flows through either the soil or the air layers is generally overlooked in addressing the SEI.

3. Energy Balance Across the Surface

We investigate the thermal energy balance within two horizontally homogeneous layers connected at a flat surface for simplicity (schematically illustrated in Figure 3): a soil layer (SL) with depth δz_s and an air layer (AL) from the surface up to z. The downward soil heat flux is measured at the bottom of the SL, $z = -\delta z_s$; turbulent heat and moisture transfers are measured at the top of the AL, z.

3.1. Thermal Energy Balance in the Air Layer

The AL includes a thin molecular diffusion layer (MDL) at the bottom of the atmosphere adjacent to the surface, which is observed by, for example, Hupfer et al. (1975) and Foken (1978), and a turbulent surface layer (TSL), which is nearly the entire AL. Although the MDL is negligibly thin, conceptually, molecular heat transfer has distinctively different characteristics from turbulent transfer in the TSL, where all measurements for studying the SEB are made.

In the TSL, the kinetic energy balance is derived from momentum conservation (e.g., Garratt, 1992). The Reynolds-decomposed kinetic energy balance in W m^{-3} with a mean variable and its perturbation represented by an over-line and a prime, respectively, can be formulated in two-dimensions for simplicity as

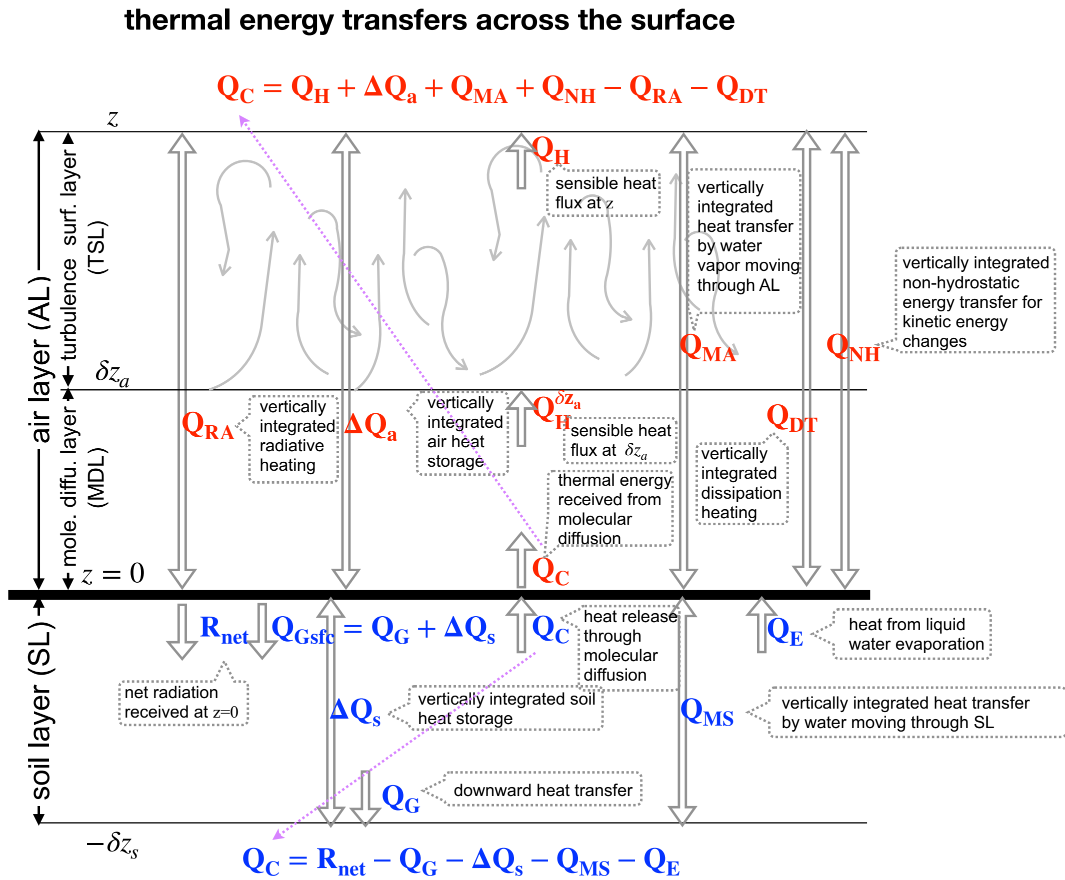

Figure 3. Schematic diagram of the thermal energy balance in the soil layer (SL, blue) and the air layer (AL, red). The soil layer is defined by the depth of the downward heat transfer Q_G at $z = -\delta z_s$; the air layer is defined by the turbulence measurement height at z, and consists of a thin molecular diffusion layer adjacent to the surface (enlarged here for visibility), and a dominant turbulent surface layer at the top. The thermal thermal energy balance in the two layers is connected through the molecular heat transfer at the surface, Q_C, that is, the blue Q_C equals the red Q_C. Under convective conditions when the mechanical forcing through the horizontal pressure gradient, radiative forcing Q_{RA}, and the thermal energy transfer due to temperature changes of water vapor passing through the AL Q_{MA} are relatively small in comparison with Q_C, Q_C is the only energy source for all the energy transfers in the AL, including heat storage ΔQ_a, the turbulent heat transfer at z, Q_H, and the vertically integrated non-hydrostatic energy transfer, Q_{NH}, for increasing kinetic energy in the AL, which is missed in the traditional thermal energy balance. The heating resulted from energy dissipation, Q_{DT}, is the by-product of the energy dissipation, which is controlled by the contribution of Q_{NH} to and the energy dissipation Q_{DK} in the kinetic energy balance (Q_{DK} is not in this diagram as this diagram is for the thermal energy balance only). In the SL, Q_{Gsfc} is added at the surface to reflect the traditional counting of the energy transfers in the SL at the surface. In reality, it represents the heat storage in the SL, ΔQ_s, and the downward heat flux, Q_G, at the bottom of the SL, which are plotted in the diagram. Note that because the liquid water evaporation, Q_E, consumes energy in the SL, thus it is blue even though the water vapor flux is estimated in the AL through the water mass balance. The additional energy transfer associated with liquid water flowing through the SL with temperature changes when it is in and out of the SL, Q_{MS}, is traditionally overlooked.

$$\overline{\rho}_a\left(\frac{\partial E_m}{\partial t} + \frac{\partial e}{\partial t}\right) = -\overline{V}\,\frac{\partial \overline{p}}{\partial x} - \overline{\rho}_a\,\frac{\partial(\overline{V}\,\overline{w'V'})}{\partial z} + \overline{q}_{NH} + \overline{\epsilon}_k, \tag{5}$$

where

$$E_m \equiv \frac{1}{2}(\overline{V}^2 + \overline{w}^2) \approx \frac{1}{2}\overline{V}^2, \tag{6}$$

$$e \equiv \frac{1}{2}(\overline{V'^2} + \overline{w'^2}), \tag{7}$$

$$\overline{\epsilon_k} \approx \mu\left[\overline{V}\frac{\partial^2\overline{V}}{\partial z^2} + \overline{V'\frac{\partial^2 V'}{\partial z^2}} + \overline{w'\frac{\partial^2 w'}{\partial z^2}}\right], \tag{8}$$

$$\overline{q}_{NH} = \overline{\rho}_a\frac{g}{\overline{\theta}}\overline{w'\theta'} - \frac{\partial\overline{w'p'}}{\partial z}. \tag{9}$$

Equation 5 includes the temporal variation (t: time) of both TKE, $\overline{\rho}_a e$, and mean kinetic energy (MKE), $\overline{\rho}_a E_m$ on the lefthand side (LHS). The two kinetic energy changes are connected through the second term on the righthand side (RHS) of Equation 5 (ρ_a: air density, V: horizontal velocity, w: vertical velocity, z: height). The first term on the RHS is the pressure gradient force (p: air pressure, x: horizontal distance). The term $\overline{\epsilon_k}$ is the kinetic energy dissipation due to the turbulent-eddy cascade resulting from the work done by the surrounding air through air dynamic viscosity, μ, and interactions between turbulence eddies and the surface.

The term $\overline{q}_{NH}$ comes from $w(\partial p/\partial z + \rho g)$ and represents the non-hydrostatic energy transfer assuming the mean state is hydrostatically balanced, which means that the vertical mean pressure gradient forcing $\overline{w}\partial\overline{p} / \partial z$ is balanced by the mean potential energy change $\overline{\rho}_a g\overline{w}$ (g: the gravity acceleration constant). Physically, the non-hydrostatic energy transfer, $\overline{q}_{NH}$, is generated in the process of restoring the atmosphere toward a new hydrostatic balance when the atmospheric hydrostatic balance is disturbed through potential energy changes as a result of vertical density fluxes. This energy transfer is responsible for thermal plumes in convection. As long as the net forcing leading the non-hydrostatic balance continues, the hydrostatic adjustment process through the vertical density flux in generating $\overline{q}_{NH}$ continues. Often, the air density is replaced with temperature and pressure through the ideal gas law, thus, $\overline{q}_{NH}$ is the sum of the two familiar terms in the TKE equation—the buoyancy generation, $\overline{\rho}_a(g / \overline{\theta})\overline{w'\theta'}$ (θ: the potential temperature), and the TKE transfer term, $\partial\overline{w'p'} / \partial z$. In investigation of the atmospheric boundary layer, only the first term is considered as an energy generation term; the second term is either parameterized in terms of heat fluxes or ignored in practice. The evidence of the role of the non-hydrostatic energy transfer due to the potential energy change in the TKE balance has been implicitly demonstrated by McBean and Elliott (1975) in their observed importance of the sum of the vertical heat flux and the vertical divergence of vertical pressure fluxes in the TKE balance.

As Bird et al. (2007) clearly stated, "there is no conservation law for internal energy." The thermal energy balance has to be derived from total energy conservation with kinetic energy conservation as the residual energy balance. Following this concept described in (Sun, 2019), which is further explained and summarized in Appendix A and also schematically illustrated in Figure 2, the thermal energy balance in W m^{-3} for the turbulent atmosphere can be expressed as

$$\overline{\rho}_a c_p\left(\frac{\partial\overline{\theta}}{\partial t} + \frac{\partial\overline{w'\theta'}}{\partial z}\right) = Q + \overline{\epsilon_t} - \overline{q}_{NH}, \tag{10}$$

where

$$\overline{\epsilon_t} \equiv \overline{\epsilon} - \overline{\epsilon_k} = \mu\left[\left(\frac{\partial\overline{V}}{\partial z}\right)^2 + \overline{\left(\frac{\partial V'}{\partial z}\right)^2} + 2\overline{\left(\frac{\partial w'}{\partial z}\right)^2}\right]. \tag{11}$$

Equation 10 is the familiar thermal energy balance except the extra term $-\overline{q}_{NH}$ (θ: potential temperature, c_p: the air specific heat at a constant pressure, Q: diabatic heating/cooling, $\overline{\epsilon_t}$: heating associated with TKE dissipation). The extra energy transfer, $-\overline{q}_{NH}$, represents the energy compensation for the consequent kinetic energy change as a result of the forcing $[Q - \nabla \cdot (p\mathbf{V}) + \epsilon]$ on a system and the non-hydrostatic adjustment in the atmosphere. That is, when the forcing Q leads to the non-hydrostatic energy transfer and kinetic energy increase, the available energy for increasing thermal energy has to be reduced to satisfy total energy conservation. Therefore, Equation 10 includes the same non-hydrostatic energy transfer $\overline{q}_{NH}$ as in Equation 5 but with the opposite sign. The traditional thermal energy balance is based on the special situation when impacts of kinetic energy changes on thermal energy changes are not considered. The heating as a result of kinetic energy dissipation, $\overline{\epsilon}_t$, represents the energy difference between the work done by the viscous stress ε in total energy conservation and the kinetic energy dissipation ϵ_k in the turbulent atmosphere (Kuo, 2005), and is well-known but often neglected in studying the atmosphere.

By vertically integrating Equation 10 in the AL to include the MDL (Appendix B), we have the thermal energy balance for the AL as

$$Q_H + \Delta Q_a + Q_{NH} + Q_{MA} = Q_C + Q_{RA} + Q_{DT}. \tag{12}$$

Equation 12 represents the balance between the energy gain/loss within the AL on the RHS and the energy consumption on the LHS. The terms in Equation 12 are the sensible heat flux at the top of the AL, Q_H, the heat storage in the AL, ΔQ_a, the vertically integrated $\overline{q}_{NH}$, Q_{NH}, the vertically integrated thermal energy change due to water vapor flux moving through the AL with its air temperature change from the surface air temperature to the air temperature at z, Q_{MA}, the molecular heat transfer at the bottom of the AL, Q_C, the vertically integrated net radiative flux divergence/convergence, Q_{RA}, and the vertically integrated heating from the TKE dissipation $\overline{\epsilon}_t$, Q_{DT}.

Alternatively, the non-hydrostatic energy transfer Q_{NH} in the AL can be estimated by vertically integrating the kinetic energy balance, Equation 5, from the surface to height z as

$$\begin{aligned} Q_{NH} &= \int_0^z \left[\overline{\rho}_a \left(\frac{\partial E_m}{\partial t} + \frac{\partial e}{\partial t} \right) + \overline{V} \frac{\partial \overline{p}}{\partial x} + \overline{\rho}_a \frac{\partial (\overline{V}\,\overline{w'V'})}{\partial z} \right] dz - \int_0^z \overline{\epsilon}_k dz, \\ &= \Delta E_k - Q_{DK}, \end{aligned} \tag{13}$$

where

$$\Delta E_k \equiv \int_0^z \left[\overline{\rho}_a \left(\frac{\partial E_m}{\partial t} + \frac{\partial e}{\partial t} \right) + \overline{V} \frac{\partial \overline{p}}{\partial x} + \overline{\rho}_a \frac{\partial (\overline{V}\,\overline{w'V'})}{\partial z} \right] dz, \tag{14}$$

$$Q_{DK} \equiv \int_0^z \overline{\epsilon}_k dz; \tag{15}$$

ΔE_k and Q_{DK} are the kinetic energy change and the energy dissipation in the AL. Equation 13 indicates that when the rate of the background mechanical work done by $\overline{V}\partial\overline{p} / \partial x$ is small, Q_{NH} would be the dominant energy source for the kinetic energy change, ΔE_k. Consequently, Q_{NH} would impact the kinetic energy transfer through momentum fluxes ($\overline{\rho}_a \partial(\overline{V}\,\overline{w'V'}) / \partial z$), the TKE dissipation ($Q_{DK} < 0$), as well as the temporal kinetic energy change.

3.2. Thermal Energy Balance in the Soil Layer

We vertically integrate the traditional thermal energy balance in the SL from $z = -\delta z_s$ to $z = 0$ (Appendix B) as the kinetic energy of the air flow in the SL is negligible,

$$R_{net} - Q_C - Q_E = \Delta Q_s + Q_G + Q_{MS} \equiv Q_{Gsfc} + Q_{MS}, \tag{16}$$

where Equation 2 is used. In Equation 16, ΔQ_s represents the heat storage of the moist soil, R_{net} is the net radiation in the SL as in Equation 1, Q_C is the heat flux exchange at the surface through molecular thermal conduction as in Equation 12, Q_G is the soil heat flux at $z = -\delta z_s$ as in Equation 1, that is, a positive Q_G represents downward heat transfer, Q_{MS} is the thermal energy flux associated with the soil water flux moving through the SL with its temperature change across the SL, and $Q_E = L_0 E$ is the latent heat flux due to liquid water evaporation E in the SL, where L_0 is the latent heat of vapourization. The thermal energy balance in the SL, Equation 16, is valid for any δz_s; however, one concern of the SL depth is the Q_G measurement accuracy, which is found to increase with increasing soil depth by Liebethal et al. (2005). Overall, Equation 16 is the same as the traditional SEB, Equation 1, except its inclusion of Q_{MS} and its explicit distinction between Q_C and Q_H, whereas $Q_C \approx Q_H$ is assumed in Equation 1.

Equation 16 indicates that Q_E in Equation 1 is the soil liquid water evaporation and a thermal energy loss in the SL even the evaporation occurs at the surface. The amount of the water loss E from the SL at the surface is commonly estimated with water vapor fluxes observed at the top of the AL, z. By doing so, the water vapor mass balance is applied with the assumption that turbulent mixing can transport water vapor effectively from the surface to the top of the AL such that the water vapor storage in the AL can be neglected. Therefore, using the turbulent moisture flux at z for estimating the water loss from the SL depends on how effective turbulent mixing in the AL is, which is discussed in Section 5.1.

3.3. Discussion of the Missing Physical Processes in the Traditional SEB Study

Although the traditional SEB may seem to deal with thermal energy transfers occurring at the surface, these transfers actually occur in either the SL or the AL. Because of the two layers share a common boundary at the surface, the surface heat transfer Q_C at the top of the SL is the same as the Q_C at the bottom of the AL. A thermal energy loss in the SL is not necessarily an energy gain is the AL. For example, the soil evaporation, Q_E, is the energy consumed for changing liquid water to water vapor in the SL. As a result of the energy balance in the SL, the soil temperature decreases. For a given air temperature over a heated surface, the reduced soil temperature would reduce the air-soil temperature difference, leading to reduced molecular thermal conduction at the surface. Consequently, the AL would receive less thermal energy from the SL instead of more. Because water vapor fluxes from the SL are estimated in the AL through the eddy-correlation method following the water mass balance, Q_E is estimated with measurements in the AL but not an energy gain in the AL; it is an energy loss in the SL. Thus, the traditional interpretation of $R_{net} - Q_{Gsfc}$ as the available energy for turbulent energy transfers $Q_H + Q_E$ in the atmosphere in the traditional formation of the SEB (Equation 3) does not correctly reflect the energy balance processes in addressing the so-called SEB.

Combining the energy balance equations in the SL and the AL, Equations 16 and 12, with the matching condition of Q_C at the surface, we have

$$\begin{aligned} R_{net} &= Q_H + Q_E + Q_{Gsfc} + \Delta Q_a + Q_{MA} + Q_{MS} - Q_{RA} - Q_{DT} + Q_{NH} \\ &\equiv (Q_H + Q_E + Q_{Gsfc}) + \Delta Q_a + Q_{res}, \end{aligned} \tag{17}$$

where

$$Q_{res} \equiv Q_{MA} + Q_{MS} - Q_{RA} - Q_{DT} + Q_{NH}. \tag{18}$$

The traditional SEB includes only the terms in the parenthesis for balancing R_{net} in Equation 17. Because the heat storage in the AL, ΔQ_a, has been considered in the literature and is generally small in the absence of plant canopies or buildings, we focus on the energy transfers in Equation 18 as the residual for the SEI investigation. Because of the appearance of Q_{NH} in both the thermal and the kinetic energy balance, $Q_{\rm res}$ can also be expressed by applying Equation 13 for $Q_{\rm NH}$ as

$$Q_{res} \equiv Q_{MA} + Q_{MS} - Q_{RA} - Q_{DT} + \Delta E_k - Q_{DK}. \tag{19}$$

Because $Q_{\rm res}$ is observed to be positive during daytime and negatively related to Q_H (Equation 3), the SEI is likely from Q_{MA}, Q_{MS}, and Q_{NH} (or ΔE_k and Q_{DK}, where $Q_{DK} < 0$) while positive Q_{RA} and Q_{DT} would contribute to the reduction of the SEI toward the SEB.

Table 1
Soil Bulk Density and In-Field Soil Moisture Calibration at the Four Stations

Variables	Station 1	Station 2	Station 3	Station 5
Elevation (m)	435.9	433.6	431.8	433.4
ρ_s ($\times 10^3$ kg m^{-3})	0.75	0.92	0.32	1.0
θ_l(obs, raw)-θ_l(lab)	0.17	0.24	0.63	0.12

4. Instrumentation and Data Processing

The field data used in this study were collected during CASES-99 (UCAR/NCAR-Earth Observing Laboratory, 2016), which was conducted in October 1999. Local standard time (LST) is 6 h behind UTC. The CASES-99 land surface was covered with short senescent grass of about 0.1 m (Sun et al., 2002, 2003, 2013). The surface observation facility consisted of a 60-m tower in the center surrounded by six stations within 300 m from the 60-m tower. On the 60-m tower, there were eight three-dimensional sonic anemometers (Campbell, CSAT version 3). The top seven levels were 5, 10, 20, 30, 40, 50, and 55 m above the surface, and the lowest one was at 1.5 and 0.5 m before and after 20 October, respectively. The lowest Krypton hygrometer (Campbell KH-20) used to measure moisture fluctuations was at 5 m. Air temperature (T_a) was measured at five samples per second with thermocouples (E-type, Chromel/Costantan) at 34 levels with the vertical resolution of 1.8 m from 2.3 to 58.1 m on the 60-m tower, and at 0.2 and 0.6 m on two adjacent poles about 1 m from the 60-m tower (Burns & Sun, 2000; Sun et al., 2002). Because of the small diameter of the thermocouple, the radiation error should be less than 0.1 K in comparison with a similar material (Figure 6.16, [Foken, 2017]). As the focus of the SEB investigation is near the surface, we assume air temperature T_a used in the study approximately equals to potential temperature θ. The Paroscientific pressure sensors were co-located with the sonic anemometer at the lowest level (0.5 or 1.5 m), 30, and 50 m, which have a resolution of 0.002 hPa with the sampling rate of 2 s^{-1} (Cuxart et al., 2002). The horizontal separation distance between the sonic anemometer and the pressure sensor at each level was about 0.2–0.3 m. Two pairs of Eppley PIR pyrgeometers for measuring upward ($L_\uparrow$) and downward ($L_\downarrow$) infrared radiation were installed at 50 m on the 60-m tower (Burns et al., 2003; Sun et al., 2003).

At each of the six surface stations, air temperature and humidity were measured by Vaisala temperature/humidity sensors at 2 m on a 10-m tower. Measurements of upward and downward longwave radiation, $L_\uparrow$ and $L_\downarrow$, with Eppley PIR pyrgeometers, and short-wave solar radiation, $S_\uparrow$ and $S_\downarrow$, with Eppley PSP pyranometers, were made at 2 m above the ground at station 2, which was about 100 m southeast of the 60-m tower. Surface radiation temperature (T_r) was measured by an Everest Interscience narrowband infrared radiometer at 10 m on each tower with 45° from nadir.

We are mainly interested in the vertical variation of net radiation in this study. Because CASES-99 was designed to investigate nocturnal boundary layers, the long-wave radiation measurements were carefully calibrated for nighttime but not for daytime (Burns et al., 2003). The absolute value of the longwave radiation measurement at a given height during daytime could be impacted by solar radiation up to about 30 W m^{-2} (Delany & Semmer, 1998). However, the vertical difference of the longwave radiation measurements should be much smaller than this value due to cancellation of similar solar radiation corrections at different observation heights.

Soil measurements were made at stations 1, 2, 3, and 5. Volumetric soil moisture at 0.025 m below the surface (θ_l. Not being confused by potential temperature used in the atmosphere) was measured continuously by Campbell CS615 water content reflectometers. Three soil samples were taken on 23 and 29 October at each station for calibrating the soil moisture sensors. The soil bulk density, ρ_s, that is, the soil weight over the total sample volume, is obtained by weighing each fresh soil sample of $0.05 \times 0.06 \times 0.06$ m and drying them in an oven. The resulting soil bulk densities at the four stations listed in Table 1 seem to be comparable with the typical bulk soil density of 1.3×10^3 kg m^{-3} (e.g., Hillel, 1998). The weight difference between the fresh and the dried sample is approximately $\rho_l\theta_l$, where ρ_l is the water density. Because the soil moisture change between 23 and 29 October was small, we averaged the laboratory-measured soil moisture over the 2 days to calibrate the field measurement at each station (Table 1). Because the soil samples might not be completely dried from the heating process, the soil water may be slightly underestimated, and the calibrated soil bulk density may be slightly overestimated. Soil temperature (T_s) was measured with NCAR soil probes inserted into the soil at an angle; thus, T_s is the averaged soil temperature from 0.01 to 0.04 m below the surface. HFT soil heat flux plates from Radiation and Energy Balance Systems, Inc. were used to measure the soil heat flux Q_G at 0.05 m below the surface. Because of instrument issues for measuring Q_G at station 1, we only use soil measurements at station 2 in this study.

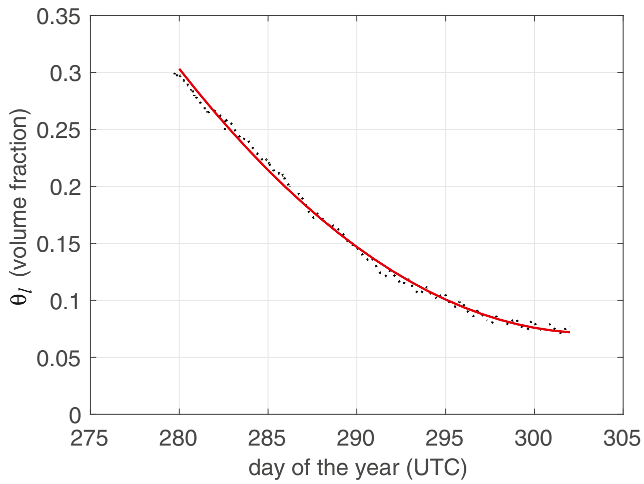

Figure 4. The time series of soil moisture θ_l at stations 2 during CASES-99, where dots are 5-min averaged data and the solid red curve is the fitted one used in this study.

A significant rain event occurred through the night of 27 September before the start of CASES-99, and there were no significant rain events during CASES-99, which is shown in the systematic decrease of the soil moisture in Figure 4. Light drizzle was reported on 8 October with no observed increase of θ_l. Dew was reported in the morning on 10 and 12 October, which was confirmed by the relatively high water vapor concentration at 2 m observed at all the stations. Because the θ_l measurement is influenced by the diurnal variation of soil temperature, the fitted temporal soil moisture curve for the entire CASES-99 at station 2 is used (Figure 4).

All the observational data are averaged over 5-min intervals. Turbulent fluxes of heat and moisture are calculated using the eddy correlation method with 5-min block averages. We find that in comparison with 30-min fluxes, the 5-min flux data set does not lead to systematic biases for the diurnal cycle of turbulent fluxes. Sensible heat flux, Q_H, is calculated using the temperature measured from the sonic anemometers because the impact of atmospheric water vapor on the sonic-anemometer temperature was relatively small during CASES-99. Only Q_H at the lowest level on the 60-m tower is used in this study. Moisture fluxes for estimating Q_E are calculated with vertical velocity (w) measurements from the sonic anemometer and specific humidity (q) from the Krypton hygrometer colocated at 5 m, which is the lowest height where fast-response moisture measurements were available. Due to the usage of specific humidity q in calculation of Q_E, no Webb correction (e.g., Webb et al., 1980) is needed (e.g., Sun et al., 1995). The impact of the path length of the sonic anemometer on turbulent fluxes at 0.5 m was investigated in Sun et al. (2013), who found that the correction is less than 4%. No attempt on various corrections on eddy correlation measurements such as those described in Oncley et al. (2007) is made because the focus of this study is the diurnal variation of the SEI and its relationship with environmental conditions not the absolute accuracy of the SEI magnitude.

Turbulent pressure fluxes $\overline{w'p'}$ at 1.5 and 30 m are also calculated by the eddy correlation method with the sampling rate of 1 s^{-1}. Because the most energetic turbulence eddies predominantly scale with observation height during daytime (Sun et al., 2016, 2020), the estimated $\overline{w'p'}$ under convective conditions should not be significantly impacted by the sampling rate. The term, $\partial\overline{w'p'} / \partial z$, is approximately estimated from the vertical difference of $\overline{w'p'}$ between 1.5 and 30 m. The detailed investigation of pressure fluxes as functions of separation distance between sonic anemometers and pressure sensors as well as atmosphere-instability is conducted by Burns et al. (2021), who found pressure fluxes are closely related to wind speed.

5. Investigation of the SEB during CASES-99

CASES-99 was not designed to investigate all the missing terms in Equation 18. Therefore, we focus our investigation on characteristics of their diurnal variations and estimate their approximate magnitudes using CASES-99 measurements that were available.

5.1. Impacts of Convective and Mechanical Turbulent Mixing on the Surface Energy Imbalance

Using the entire CASES-99 data set, we find that on average, Q_{res} are closely related to the air-surface temperature difference, $\overline{T}_r - \overline{T}_a(2.3\text{ m})$, where $\overline{T}_a(2.3\text{ m})$ represents the air temperature at $z = 2.3$ m (Figure 5a). It is shown in Figure 5a that Q_{res} increases sharply with $\overline{T}_r - \overline{T}_a(2.3\text{ m})$ for $\overline{T}_r - \overline{T}_a(2.3\text{ m}) > 0$, approaches zero when $\overline{T}_r - \overline{T}_a(2.3\text{ m}) \approx 0$, and decreases gradually with decreasing $\overline{T}_r - \overline{T}_a(2.3\text{ m})$ for $\overline{T}_r - \overline{T}_a(2.3\text{ m}) < 0$. This result is consistent with the observed diurnal variation of Q_{res} in Figure 1, where Q_{res} is plotted as negative as Q_H is plotted as positive.

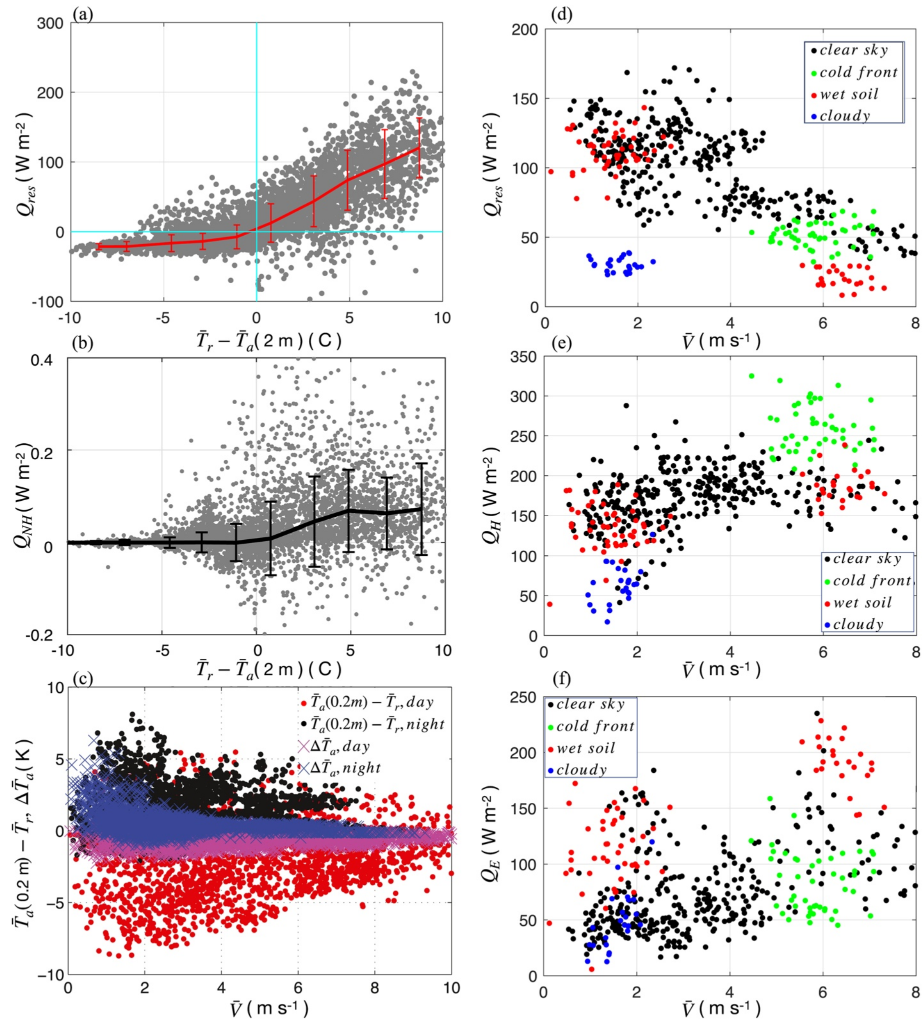

Figure 5. Observed relationships between the surface-air temperature difference, $\overline{T}_r - \overline{T}_a(2\ \mathrm{m})$, and (a) Q_{res} and (b) Q_{NH}. (c) Relationships between wind speed $\overline{V}$ at the lowest sonic anemometer level (1.5 or 0.5 m), the air-surface temperature difference $\overline{T}_a(0.2\ \mathrm{m})$–$\overline{T}_r$, and the vertical air temperature difference $\Delta\overline{T}_a = \overline{T}_a(0.6\ \mathrm{m})$–$\overline{T}_a(0.2\ \mathrm{m})$. Relationships between $\overline{V}$ and (d) Q_{res}, (e) Q_H, and (f) Q_E around noon (1100 LST–1300 LST), where $\overline{V}$, Q_{res}, and Q_H are measured at the lowest sonic anemometer height, and Q_E is measured at 5 m. The thermocouple measurement is used for $\overline{T}_a$. Each dot represents a 5-min averaged value in (a–c), and a 25-min averaged value in (d–f) for easy view. In (a and b), the thick curves represent the bin-averaged relationships and the vertical thin lines represent the standard deviations of the points within each horizontal bin. In (d–f), the conditions for a cold front, the relatively high soil moisture at the beginning of CASES-99, and the cloudy day of 8 October as well as the rest of clear sky days are marked in green, red, blue, and black. In (c), the day and night times are defined as the positive and negative net radiation, respectively. Note that the magnitude of Q_{NH} in (b) is significantly underestimated due to the lack of direct measurements near the surface; however, its diurnal variation is found invariant with height under free convective conditions. Thus, the dependence of Q_{NH} on $\overline{T}_r - \overline{T}_a(2\ \mathrm{m})$ in (b) is found to be consistent with that of Q_{res} in (a).

We further explore the dependence of Q_{res} on atmospheric stratification through examining how Q_{res} varies with $\overline{V}$ at 1.5 m around noon (between 1100 LST and 1300 LST) when $\overline{T}_r - \overline{T}_a(2.3\ \mathrm{m})$ reaches its potential maximum value. Based on Sun et al. (2016, 2020), the variation of the atmospheric surface-layer stratification is correlated with wind speed $\overline{V}$. Strong shear-generated turbulent mixing associated with strong winds can effectively mix the air near the surface to its neutral state regardless of surface heating/cooling. Thus, stable or unstable stratification can only occur under weak winds, which is evident in Figure 5c and in Foken (1978). We find that Q_{res} around noon decreases approximately linearly with $\overline{V}$ (Figure 5d) except under cloudy conditions, which is consistent with the approximate increase of both Q_H and Q_E with $\overline{V}$ (Figures 5e and 5f) as Q_{res} is negatively related with Q_H and Q_E (Equation 3). Under cloudy conditions, $\overline{T}_r$ is not much higher than $\overline{T}_a$(2.3 m) even under weak winds, corresponding to near neutral conditions; thus, Q_{res} is relatively small. As strong winds correspond to large friction velocity (Sun et al., 2016, 2020), the decrease of Q_{res} with $\overline{V}$ is consistent with the observed relationship between Q_{res} and friction velocity u_* in the literature (e.g., Barr et al., 2006; Mauder et al., 2018; Nelli et al., 2020; Oliphant et al., 2004; Sánchez et al., 2010; Wilson et al., 2002).

The observed correlations between Q_{res}, $\overline{T}_r - \overline{T}_a$(2.3 m), and $\overline{V}$ clearly indicate that convective turbulent mixing does not remove the warm and moist air away from the surface as effectively as mechanically generated turbulent mixing does. The role of mechanically generated turbulence in the SEI was also discussed by Hendricks Franssen et al. (2010) and Zhou et al. (2018). The negative correlation between the thickness of the estimated molecular diffusion layer depth and wind speed was indeed observed by Hupfer et al. (1975) and Foken (1978). The reasonably robust relationships between Q_{res}, $\overline{T}_r - \overline{T}_a$(2.3 m), and $\overline{V}$ for the entire CASES-99 regardless of wind direction, temperature advection, and mesoscale circulations confirm the studies in the literature that temperature advection (Leuning et al., 2012; Oliphant et al., 2004) and mesoscale circulations (e.g., Steinfeld et al., 2007) are not persistent factors in explaining the systematic diurnal variation of the SEI.

To further explore why the largest SEI is associated with free convective conditions, we explore how heat fluxes vary vertically near the surface by examining temperature standard deviation σ_θ using thermocouple temperature measurements. Because of $\overline{w'\theta'} \equiv -u_*\theta_*$ and the observed linear relationship between θ_* and σ_θ at a given z under convective conditions (Figure 6a), $\overline{w'\theta'}$ would vary linearly with σ_θ if u_* is approximately invariant with z near the surface, which was examined in Sun et al. (2013). By compositing σ_θ at 0.5 and 1.5 m for the daytime CASES-99 data, we find that, on average, σ_θ increases with net radiation, R_{net}, and decreases with height (Figure 7d). The observed characteristics of σ_θ suggest that on average, the heat flux reaches its daily maximum around noon, decreases with height, and the heat flux convergence reaches its maximum around noon, which is consistent with the observed heat flux decrease with height based on the direct eddy correlation measurements of Q_H at 0.5 and 1.5 m as functions of R_{net} (Figure 6b). Considering the daily maximum downward solar radiation decreases with time in October during CASES-99 (Figure 6c) and the sonic anemometer at 1.5 m was moved to 0.5 m during the last half of CASES-99, the vertical decrease of the observed heat flux with R_{net} would be even larger than it is in Figure 6b. Because convective turbulence eddies transport both heat and moisture, and Q_E increases with surface humidity q (estimated as q at 2 m around 0600 LST before the daytime convection starts) for a given Q_H (Figure 6d), Q_E is expected to decrease with height as well during daytime.

To explore impacts of thermally and mechanically generated turbulent mixing on the heat transfer, we focus on 2 days: 10 October when the wind was the weakest corresponding to the most convective day during CASES99, and 15 October when the wind was nearly the strongest during CASES-99 and turbulent mixing was dominated by mechanically generated turbulence eddies (Figure 7e). The two days had similar downward solar radiation (Figure 6c), however, the surface radiation temperature $\overline{T}_r$ and the downward heat transfer in the soil Q_G were higher during the convective day than the windy day (Figures 7b and 7f), suggesting that heat from the surface was not effectively transferred to the air during the convective day in comparison with the windy day. In addition, we find that σ_θ decreased sharply with z below 5.9 m (Figure 7d) and changed little with z above (not shown) on the convective day and nearly invariant with height on the windy day (Figure 7h). Considering the relatively homogeneous surface at the observation site, the impact of the changing footprint with height on σ_θ should be small, which is evident in the relatively symmetric diurnal variation of σ_θ around noon in spite of the changing solar zenith angle during the day. The sharp decrease of σ_θ with height implies that $\overline{w'\theta'}$ decreased significantly with height on the convective day, and was nearly invariant with height only on the windy day, which contradicts the notion that the surface layer is a constant-flux layer under all conditions. As a result, the air temperature decreased with height more significantly on the convective day than on the windy day (Figures 7a, 7c, and 7g). Consequently, Q_{res} was much smaller around noon on the windy day when heat and moisture are more effectively transferred by mechanical turbulence from the surface up to the turbulence measurement height z than on the convective day (Figure 8a).

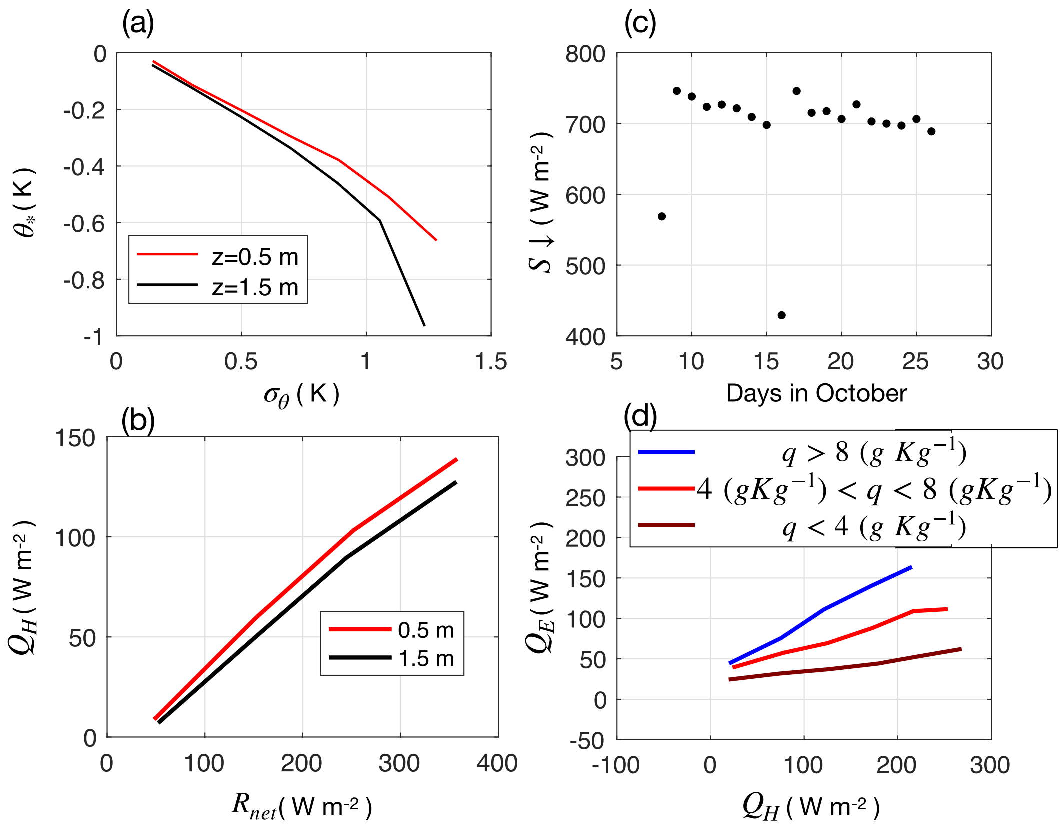

Figure 6. The composite relationships (a) between 5-min standard deviation of thermocouple temperatures σ_θ and θ_* and (b) between sensible heat fluxes Q_H at 0.5 and 1.5 m and net radiation R_{net} based on the daytime data from the entire field campaign. (c) The time series of the maximum downward solar radiation at 2 m, station 2, $S\downarrow$, during the field campaign in October 1999. (d) The daytime relationship between Q_H and Q_E at 5 m for three 2-m specific humidity categories: $q > 8$ g kg^{-1}, 4 g kg^{-1} $< q <$ 8 g kg^{-1}, and $q <$ 4 g kg^{-1} around 0600 LST at station 1.

The above observational results demonstrate that thermally and mechanically generated turbulent mixing transfers heat and moisture differently. Because thermally generated turbulent mixing is maintained by positive buoyancy, the warm air near the surface cannot be completely transferred to the turbulent flux measurement height. Mechanically generated turbulent mixing, on the other hand, relies on bulk wind shear, that is, $\overline{V}$ at z, and can effectively reduce the surface-layer stratification, leading to the efficient heat and moisture transfer of the surface air up to z. When the surface and the air temperatures are approximately the same, such as around sunrise and sunset when the surface is between being the heat source and being the heat sink to the atmospheric boundary layer (e.g., Foken, 2008; Oncley et al., 2007) or when the surface is wet (e.g., Eder et al., 2014; Mauder et al., 2007), molecular heat transfer would be effectively zero. That is, without the surface heat source/sink for the atmospheric surface layer, the air near the surface would be near neutral, and the turbulent heat flux would be zero as well. Under this neutral situation, the turbulent heat flux is the same as the molecular heat transfer, and the resulting Q_{res} is zero as well.

The above observational analysis also indicates that the surface energy is balanced under two conditions. One is when the AL is neutral with no heat added into or removed from the AL such as when R_{net} is zero; the other is when warm or cold air from the surface is effectively transferred vertically by strong mechanically generated turbulent mixing under strong winds even when surface heating/cooling is present. Therefore, the major issue for the SEI is related to the atmospheric stratification, especially under convective conditions. Knowing that $\overline{w'\theta'}$ decreases with z significantly near the surface on the strong convective day and assuming that $\partial\overline{w'\theta'}$ / ∂z varies linearly with $\partial\sigma_\theta/\partial z$, the estimated $\overline{w'\theta'}$ at 0.2 m would be about 1.7 times the directly measured $\overline{w'\theta'}$ at 1.5 m. Using this estimated Q_H closer to the surface for a closer assessment of Q_C alone, the estimated Q_{res} would be reduced to across the zero line (Figure 8a).

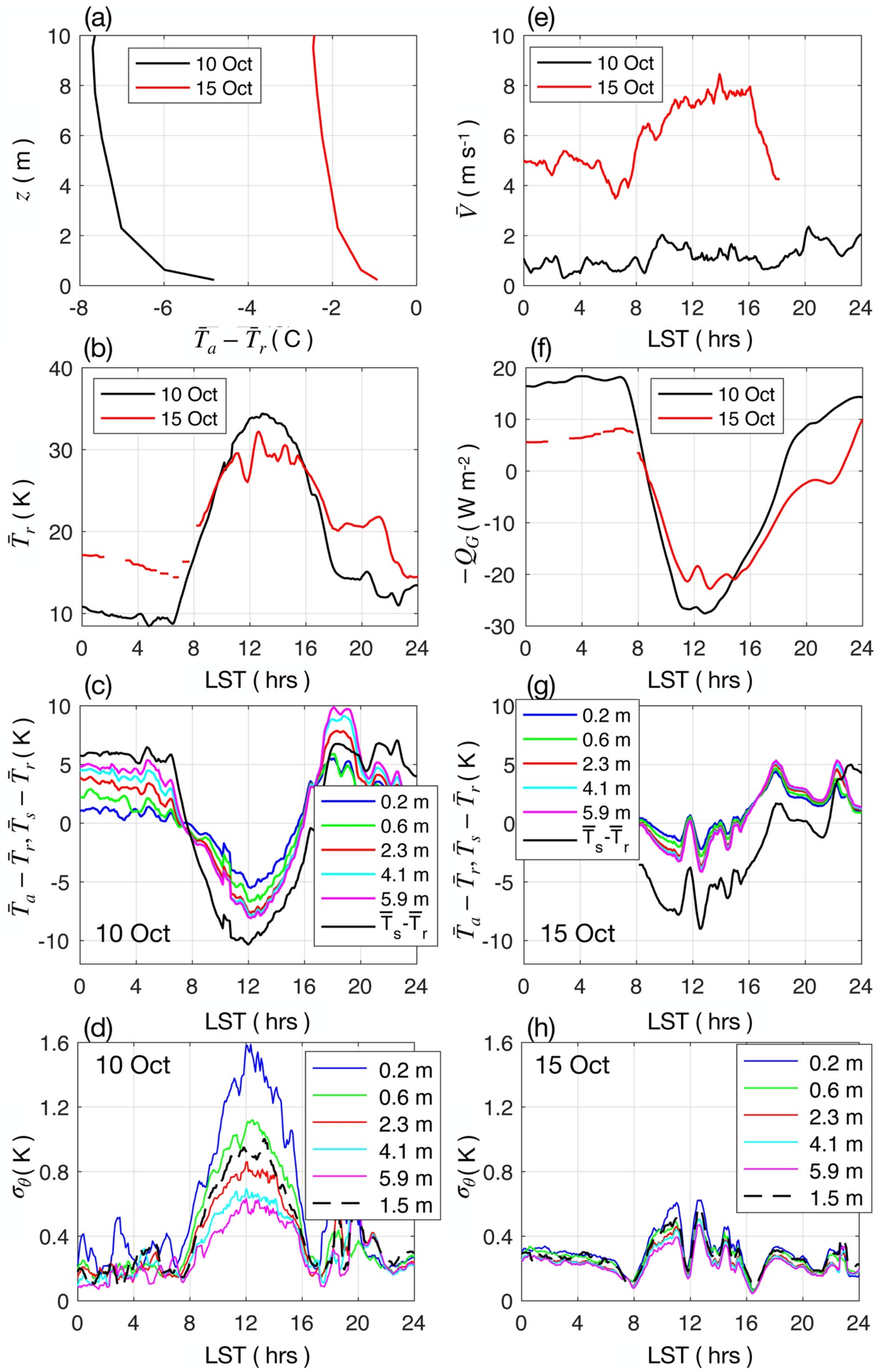

Figure 7. Comparisons of thermodynamic structures near the surface as a result of turbulence eddies generated by strong thermal forcing (weak wind, 10 October) and by mechanical forcing (strong wind, 15 October). (a) The vertical profiles of the averaged thermocouple air temperature $\overline{T}_a$ relative to the surface radiation temperature $\overline{T}_r$ around noon (1100–1300 LST). The temporal variations of (b) $\overline{T}_r$, (c and g) the air-surface temperature difference, $\overline{T}_a - \overline{T}_r$ with $\overline{T}_a$ at the labeled levels, (d and h) the 5-min temperature standard deviations σ_θ from the thermocouple temperature measurement at the labeled levels, (e) the wind speed at 1.5 m, $\overline{V}$, and (f) the downward heat transfer in the SL, Q_G. In addition, the soil temperature between 0.01 and 0.04 m below the surface relative to $\overline{T}_r$ is plotted in (c) and (g); σ_θ from the 1.5-m sonic anemometer at 1.5 m is plotted in (d and h) for comparison. Comparisons between (c and g) and between (d and h) indicate that heat fluxes vary significant with height near the surface under free convective conditions, implying that mechanically generated turbulent mixing is more effective in transferring heat from the surface upward than positive buoyancy generated turbulent mixing.

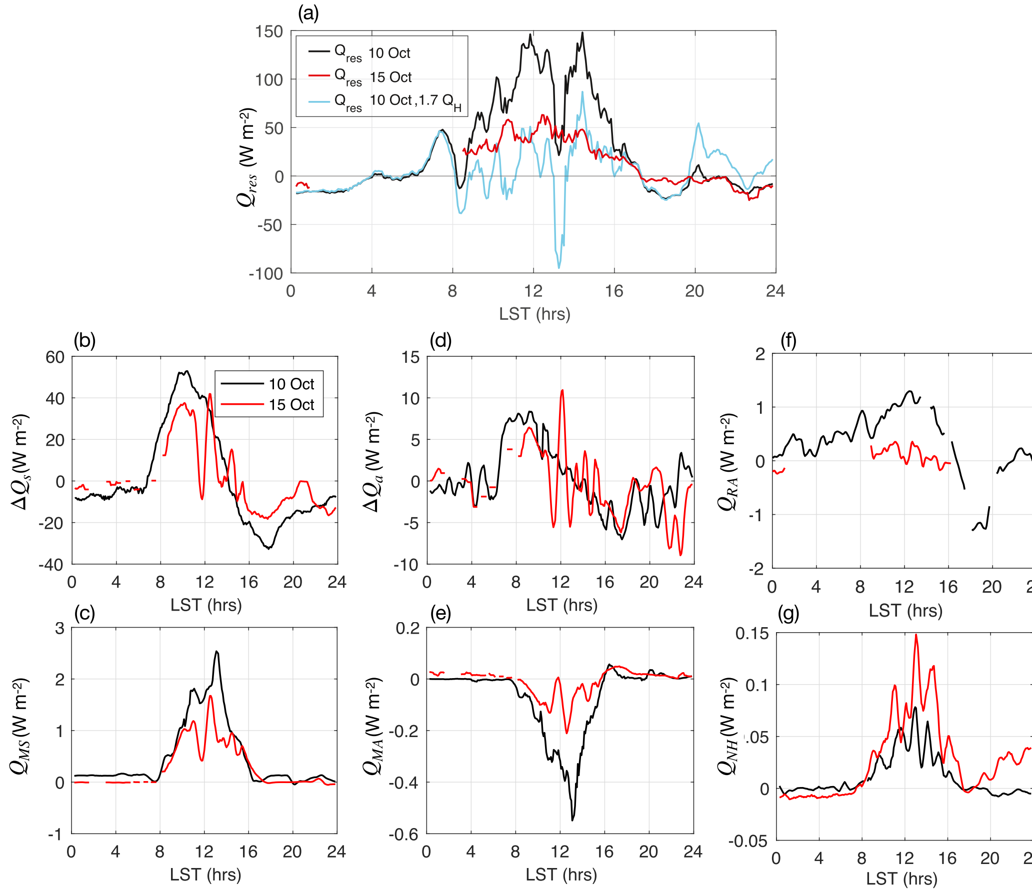

Figure 8. The diurnal variations of (a) the surface energy imbalance, Q_{res}, estimated with Q_H observed at 1.5 m, (b) ΔQ_s, (c) Q_{MS}, (d) ΔQ_a, (e) Q_{MA}, (f) Q_{RA}, and (g) the direct estimate of Q_{NH} based on the available observations for the convective day, 10 October, and the windy day, 15 October. In (a), Q_{res} estimated with 1.7 times the observed Q_H on the convective day for a better estimate of Q_C is also plotted in cyan, suggesting that an improved estimate of Q_C would reduce the systematic surface energy imbalance. Due to the lack of measurements near the surface in the AL where heat and moisture fluxes vary significantly with height under free convective conditions, we mainly focus on the temporal variations of Q_{MS}, Q_{MA}, and Q_{NH}. The magnitude of Q_{NH} is also estimated using the kinetic energy balance as explained in the text, which indicates that Q_{NH} is significantly underestimated with measurements far above the surface.

5.2. Estimation of Surface Energy Imbalance Under Convective Conditions

Knowing that the SEI is the largest under convective conditions, we investigate where the thermal energy Q_C goes to in the AL through analyzing all the missing terms that contribute to Q_{res} in Equations 18 and 19, and their variations with R_{net} on the convective day of 10 October in this subsection. Because Q_G was measured at $z = -0.05$ m, the lowest moisture flux measurement height was at 5 m, and the lowest level for heat flux measurements was below 5 m, we consider the top 0.05-m soil layer as the SL, that is, $\delta z_s = 0.05$ m, and the air layer above the surface up to 5 m as the AL.

We first estimate the diurnal variation of Q_{RA} in comparison with Q_{res} as radiation divergence measurements are rare. Due to the lack of observations for vertical variations of shortwave radiation, the longwave radiation measurements are available only at two heights, 2 and 50 m, which is much deeper than the AL, and the longwave calibration was performed for nighttime even though its impacts of the calibration on the vertical difference between two levels could be relatively small, we only approximately estimate the longwave contribution of Q_{RA} by assuming $Q_{RA} \simeq (L_{\uparrow}^{2\,m} - L_{\downarrow}^{2\,m} - L_{\uparrow}^{50\,m} + L_{\downarrow}^{50\,m})z\,/\,(50-2)$. We find that the diurnal variation of the longwave part of Q_{RA} on the convective day is not consistent with that of Q_{res} (Figures 8a and 8f).

5.2.1. Thermal Energy Transfer by Water Mass Flow

Thermal energy changes associated with water flows in the SL, Q_{MS}, and with water vapor fluxes in the AL, Q_{MA}, are overlooked in the traditional SEB as we are not used to consider an open system with moving water mass although its impact on the soil thermal energy balance has been investigated in the literature (e.g., Bredehoeft & Papaopulos, 1965; De Vries, 1958; Gao et al., 2007; Milly, 1982; Milly & Eagleson, 1980; Shao et al., 1998; Sun et al., 1995; Van Orstrand, 1934). De Vries (1958) combined Q_{MS} and Q_E as LE where $L \equiv L_0 - (c_{pl} - c_{pv})(T_s - T_0)$, c_{pl} and c_{pv} are the heat capacities for liquid water and water vapor, and T_0 was defined as a reference temperature. With the assumption of a constant L, the energy transfer through water fluxes with the temperature change of $(T_s - T_0)$, Q_{MS}, is often forgotten. Philip (1957) assumed that soil temperature gradients are unimportant in the soil water mass balance, and implicitly assumed that soil temperature gradients are also unimportant in the thermal energy transport associated with moving water, which is Q_{MS}.

The thermal energy associated with water flow, Q_{MS} in the SL, and Q_{MA} in the AL can be estimated by using the observed temporal variation of soil moisture $\partial\theta_l/\partial t$, evaporation E with the water mass conservation equation, and temperature measurements in the SL and the AL (Equations B19 and B20 in Appendix B). We estimate the temporal variation of soil moisture, $\partial\theta_l/\partial t$, by using the fitted temporal curve of θ_l during the entire CASES-99 at station 2. Assuming $E \approx \overline{\rho}_a \overline{w'q'}(z)$ (Equation B20 in Appendix B), we find that both Q_{MS} (Equation B17 in Appendix B) and Q_{MA} (Equation B7 in Appendix B) vary with the downward solar radiation and reach their maxima of 2.5 Wm^{-2} for Q_{MS} and about -0.5 Wm^{-2} for Q_{MA} around noon on the convective day and less on the windy day (Figures 8c and 8e). Because of the accumulation of water vapor near the surface under convective conditions, $E \approx \overline{\rho}_a \overline{w'q'}(z)$ would underestimate the amount of water vapor coming out of the surface on the convective day, leading to underestimation of both Q_{MS} and Q_{MA}. In addition, without measurements of the soil temperature at $-\delta z_s$ and without knowing where the evaporation occurs in the SL, we cannot accurately estimate the vertical temperature difference in estimating Q_{MS}. Because the liquid water heat capacity is about two times larger than the water vapor heat capacity, the liquid water density is about 10^6 times larger than the water vapor density with $q = 10$ g kg^{-1}, and the vertical temperature difference across the SL is O(10) K, Q_{MS} is about O(10) Wm^{-2} and much larger than Q_{MA}. Because Q_{MS} has the same diurnal variation as Q_{res} does and is positively related to Q_{res}, it represents an extra energy transfer contributing to Q_{res}. The magnitude of Q_{MS} needs to be further investigated with adequate measurements. Nonetheless, the magnitude of Q_{MS} is much smaller than the overall imbalance of O(100) Wm^{-2} under convective conditions.

5.2.2. Daytime Non-Hydrostatic Energy Transfer

We first explain physical processes related to Q_{NH} and the diurnal correlation between Q_{NH} and Q_{res}. As the air temperature near the surface increases through the molecular heat transfer Q_C at the surface, the surface air expansion leads to the air density decrease near the surface below the relatively high density air, or positive buoyancy under the influence of gravity. The positive buoyancy results in negative air density fluxes and potential energy decrease. Part of the potential energy change could be balanced with the variation of the vertical pressure gradient forcing, that is, the mean hydrostatic balance. The rest of the potential energy change would result in hydrostatic imbalance of the air layer, leading to non-hydrostatic energy transfer, that is, positive Q_{NH} in the kinetic energy balance (Equation 5). The increase of TKE associated with positive buoyancy is evident in the commonly observed development of thermal plumes. As a consequence of the contribution of the surface heating to the TKE increase through the non-hydrostatic energy transfer Q_{NH}, the available energy for the thermal energy transfer in the AL would be reduced by Q_{NH}, resulting in smaller Q_H at the top of the AL than it could be without the non-hydrostatic energy transfer. The reduced Q_H would contribute to the observed positive Q_{res} (Equation 18) as observed in Figure 8a. When the surface is cooled at night, air compression contributes to a surface air density increase and stable atmospheric stratification. Shear generated large turbulence eddies have to lift high density cold air upward and push low density warm air downward, resulting in positive vertical density fluxes at the expense of the reduced potential TKE increase. Again, the hydrostatic balance would be disturbed through the potential energy increase caused by positive vertical density fluxes, leading to a negative non-hydrostatic energy transfer, that is, $Q_{NH} < 0$. As a result, the AL would cool less than what the thermal energy sink Q_C provides. The negative Q_{NH} is consistent with the observed negative Q_{res} at night (Figure 8a). When the air temperature is equal to the surface

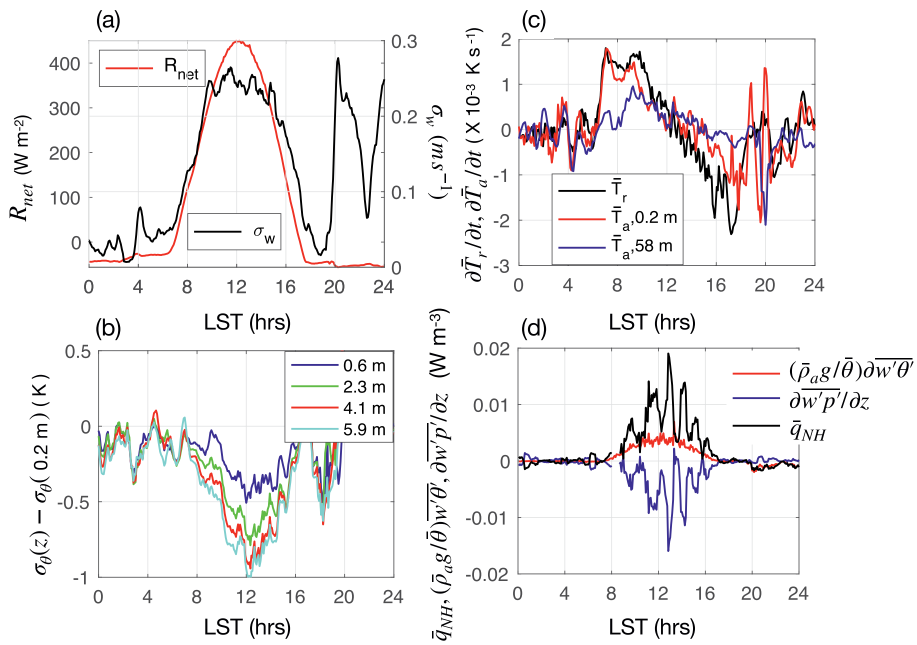

Figure 9. Diurnal variations of (a) net radiation R_{net} and the 5-min standard deviation of vertical velocity σ_w at 1.5 m, the temporal variations of (b) the 5-min standard deviations of the thermocouple air temperature σ_θ relative to σ_θ at 0.2 m at the labeled heights, (c) $\overline{T}_r$ and $\overline{T}_a$ at 0.2 and 58 m, and (d) the diurnal variations of $\overline{q}_{NH}$ and its two terms, $(\overline{\rho}_a / g)\overline{w'\theta'}$ and $\partial\overline{w'p'} / \partial z$ for the convective day, 10 October. Note that the different temporal variations between $\partial\overline{T}_a / \partial t$ and $\partial\overline{w'\theta'} / \partial z$ suggested by the vertical difference of σ_θ indicate that the traditional thermal energy balance is not valid; the simultaneous decrease of the temporal variation of $\partial\overline{T}_a / \partial t$ near the surface and the increase of $\overline{q}_{NH}$ around 8 LST indicate that the non-hydrostatic energy transfer $\overline{q}_{NH}$ for kinetic energy increase due to the surface heating contributes to the slow-down of the air temperature increase in the morning suggested by total energy conservation.

temperature or when the AL is well mixed by mechanically generated turbulent mixing under strong winds, the air density is approximately invariant with height so that the vertical air density flux and Q_{NH} would be zero, which is consistent with the observed zero Q_{res}. Therefore, qualitatively, the diurnal variations of Q_{NH} and Q_{res} are positively correlated.

5.2.2.1. Direct Estimation of Non-Hydrostatic Energy Transfer

We first study the non-hydrostatic energy transfer at a given point, $\overline{q}_{NH}$ in Equation 9, based on direct observations of the two terms in $\overline{q}_{NH}$, $(\overline{\rho}_a / g)\overline{w'\theta'}$ and $\partial\overline{w'p'} / \partial z$ with emphasis on their daytime variations with the downward solar radiation as we do not have adequate observations for estimating the magnitudes of both terms within the desired AL of 5 m. With the available observation of $\overline{w'p'}$ at 1.5 and 30 m, we find that $\overline{w'p'}$ is negative at both levels, their magnitudes all appear to be largest around noon (not shown), resulting in the largest negative $\partial\overline{w'p'} / \partial z$ around noon on the convective day (Figure 9d). Using the 5-min data during the entire field campaign, we find that the standard deviation of the vertical velocity σ_w is systematically related to σ_p and $\partial\overline{w'p'} / \partial z$ day and night (the composite lines in Figures 10b and 10d) while the relationships between σ_w and σ_θ as well as between σ_w and $(\overline{\rho}_a g / \overline{\theta})\overline{w'\theta'}$ vary significantly between day and night (Figures 10a and 10c). That is, in comparison with large diurnal variations of $\overline{w'\theta'}$, $\partial\overline{w'p'} / \partial z$ plays a consistent role in generating TKE changes day and night, which was also observed by McBean and Elliott (1975). Due to a lack of observations of $\overline{w'p'}$ in most of field campaigns, the contribution of $\partial\overline{w'p'} / \partial z$ to TKE changes is often parameterized based on $\overline{w'\theta'}$ or ignored in the literature, which may present problems based on the observations in Figure 10. As both $(\overline{\rho}_a g / \overline{\theta})\overline{w'\theta'}$ at 1.5 m and $-\partial\overline{w'p'} / \partial z$ between 1.5 and 30 m maximize at noon, the vertically integrated $\overline{q}_{NH}$, Q_{NH}, also maximizes at noon (Figure 8g), which confirms the diurnal relationship between Q_{NH} and Q_{res}. Considering the significant vertical variation of the sensible heat flux near the surface as explained in Section 5.1 and possibly similar vertical variations of $\partial\overline{w'p'} / \partial z$, the

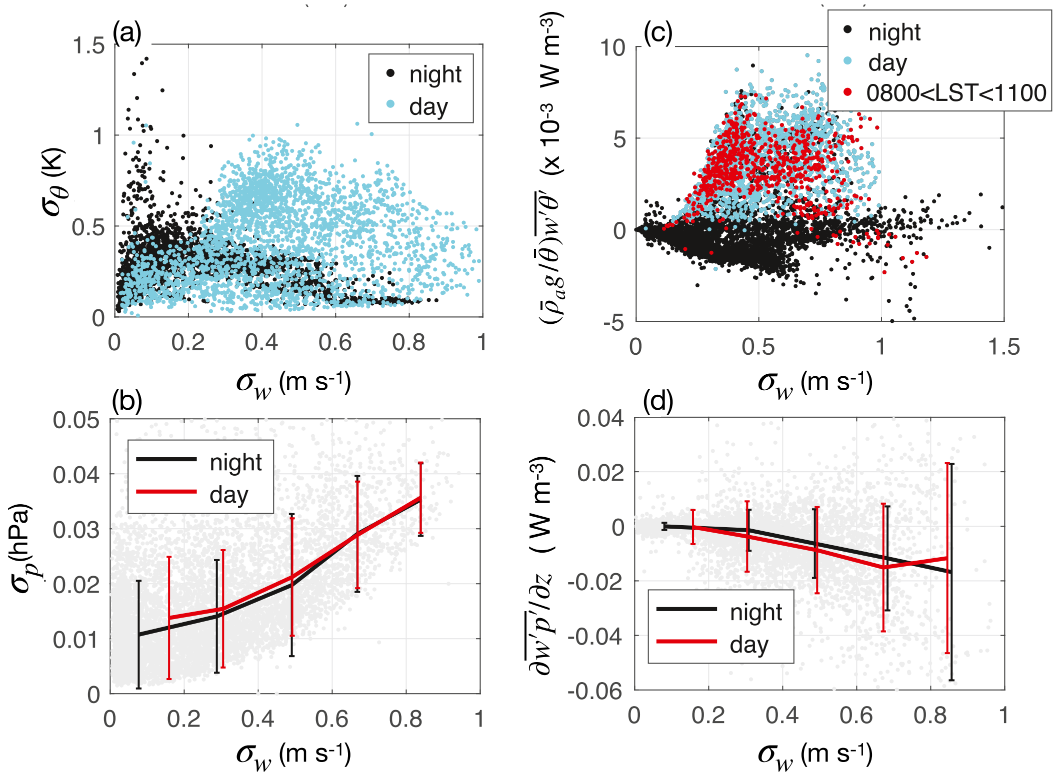

Figure 10. Relationships between the 5-min standard deviation of vertical velocity σ_w at its lowest observation height and (a) the 5-min standard deviation of temperature, σ_θ, (b) the 5-min standard deviation of pressure, σ_p, (c) $(\overline{\rho}_a g \, / \, \overline{\theta})\overline{w'\theta'}$, and (d) $\partial\overline{w'p'} \, / \, \partial z$ during the entire CASES-99, where $\partial\overline{w'p'} \, / \, \partial z$ is estimated using the $\overline{w'p'}$ measurements at 1.5 and 30 m. Each dot represents a 5-min data point. Although the scatter of each panel is relatively large as the entire CASES-99 data set is included, the relationships between σ_w, σ_p, and $\partial\overline{w'p'} \, / \, \partial z$ are consistent day and night in comparison with σ_θ and $(\overline{\rho}_a g \, / \, \overline{\theta})\overline{w'\theta'}$. The results indicate that the contribution of pressure fluxes, which is often neglected or parameterized with heat fluxes, is important in the non-hydrostatic energy transfer and may vary differently from heat fluxes.

magnitude of Q_{NH} in Figure 8g is significantly underestimated. The magnitude of Q_{NH} is further indirectly estimated using Equation 13 next.

Based on the observed temporal variation of $\overline{q}_{NH}$ under convective conditions, we can further confirm the role of $\overline{q}_{NH}$ in the thermal energy balance. On the convective day, the diurnal variation of $\overline{T}_r$ follows the diurnal variation of R_{net}; the largest $\partial\overline{T}_r \, / \, \partial t$ is around 0800 LST. At 0.2 m, $\partial\overline{T}_a \, / \, \partial t$ follows closely with $\partial\overline{T}_r \, / \, \partial t$, whereas at 58 m $\partial\overline{T}_a \, / \, \partial t$ reaches its maximum several hours later (Figure 9c). Meanwhile, $\partial\overline{w'\theta'} \, / \, \partial z$ maximizes around noon based on the observed $\partial\sigma_\theta/\partial z$ (Figure 9b). The temporal mismatch between the diurnal variations of $\partial\overline{T}_a \, / \, \partial t$ and $\partial\overline{w'\theta'} \, / \, \partial z$ indicates that $\partial\overline{w'\theta'} \, / \, \partial z$ is not the only energy source for the air temperature change as expected in the traditional thermal energy balance when temperature advection is negligible, which is the case on the convective day. The perfect timing between the $\overline{q}_{NH}$ increase and the $\partial\overline{T}_a \, / \, \partial t$ decrease in Figures 9c and 9d indicates that the decrease of $\partial\overline{T}_a \, / \, \partial t$ is indeed due to the non-hydrostatic energy transfer. When vertical air density fluxes are negligibly small such as in the SL, $\overline{q}_{NH}$ would be approximately zero. Using soil and air temperature measurements with the assumption that the soil temperature at the top of the SL and the bottom of the AL are the same as the surface radiation temperature $\overline{T}_r$, we find that ΔQ_s peaks around noon whereas ΔQ_a peaks in the morning on the convective day (Figures 8b and 8d). Thus, indeed the diurnal variations of the soil heat flux, Q_G, and ΔQ_s are approximately in phase. Therefore, the different relationships between the temporal variation of $\overline{T}_a$ and the turbulent heat transfer in the AL, $\overline{w'\theta'}$, and between the temporal variation of $\overline{T}_s$ and the soil heat transfer, Q_G, further illustrate the important role of the non-hydrostatic energy transfer in the atmospheric thermal energy balance explained in Sun (2019) and Appendix A.

5.2.2.2. Indirect Estimation of the Magnitude of Non-Hydrostatic Energy Transfer

We investigate the possible magnitude of Q_{NH} through kinetic energy conservation Equation 13 by focusing on the convective day. Because the weak wind was steady throughout the convective day, the contribution of horizontal pressure gradients to MKE and TKE changes has to be relatively small, and the temporal variation of kinetic energy $\partial e/\partial t$ has to be from the non-hydrostatic energy transfer as demonstrated in the close relationship between R_{net} and σ_w (Figure 9a). Because e reaches its maximum around noon, $\partial e/\partial t$ would reach its maximum in the morning. Meanwhile, the kinetic energy dissipation $\overline{\epsilon_k}$ is proportional to e, thus, $\overline{\epsilon_k}$ is the only term in the kinetic energy balance that has the same diurnal variation as $\overline{q}_{NH}$ does on the convective day. That is, Q_{res} can be directly related to Q_{DK} as indicated in Equation 19.

We first study the dependence of $\overline{\epsilon_k}$ on atmospheric instability in comparison with the observed Q_{res} before we investigate the magnitude of Q_{NH}. We examine the vertical variation of the normalized vertical velocity spectrum $2\pi f S_w \,/\, \sigma_w^2$ (S_w is the power spectrum of w and f is frequency) as a function of non-dimensionalized frequency $2\pi fz/V$ for the convective day in comparison with the windy day (Figures 11a and 11c). We find that the normalized high-frequency w spectrum increases toward the surface on the convective day, suggesting that high frequency turbulence intensity increases toward the surface. That is, the inertial subrange of the w spectrum would shift toward higher frequency as the observation height decreases. Based on the Kolmogorov law, $\overline{\epsilon_k}^4$ is inversely related to Kolmogorov's microscale in the inertial subrange. The shift of the inertial subrange for the w spectrum toward high frequency implies $\overline{\epsilon_k}$ increasing toward the surface. In contrast, the normalized spectrum on the windy neutral day remains unchanged with height, implying $\overline{\epsilon_k}$ is nearly invariant with height under neutral conditions.

We then study the vertical variation of $\overline{\epsilon_k}$ based on its analytic formula, Equation 8. Assuming $\overline{\epsilon_k}$ is dominated by vertical variations of mean wind $\overline{V}$, and $\overline{V}$ varies log-linearly with height as $\overline{V} = u_* \ln(z \,/\, z_o)$ under free convective conditions, where z_o is the roughness length, and u_* is the friction velocity observed at noon on the convective day, $\overline{\epsilon_k} \,/\, \mu$ would increase toward the surface logarithmically as shown in Figure 11d. The dramatic increase of $\overline{\epsilon_k}$ toward the surface has indeed been observed, for example, by Lenschow et al. (1988).

We then estimate $\overline{\epsilon_k}$ as a function of atmospheric stability based on published studies in the literature. The increase of the non-dimensionalized $\overline{\epsilon_k}$, $\kappa z\overline{\epsilon_k} \,/\, u_*^3$, as a function of instability $-z \,/\, L = -\kappa z(g \,/\, \overline{\theta})(\theta_* \,/\, u_*^2)$ (κ is the von Kármán constant, L is the Obukhov length, and $\overline{\theta}$ is a reference potential temperature) has been studied with field measurements (e.g., Albertson et al., 1997; Charuchittipan & Wilson, 2009; Wyngaard & Cotè, 1971). Both Wyngaard and Cotè (1971) (hereinafter WC) and Albertson et al. (1997) (hereinafter APKE) found that $\kappa z\overline{\epsilon_k} \,/\, u_*^3$ increased significantly with increasing instability $-z/L$ based on field observations at 3 m above the surface (Figure 11b). Charuchittipan and Wilson (2009) demonstrated that among all the observed $\kappa z\overline{\epsilon_k} \,/\, u_*^3$ as a function of $-z/L$, its increase is least for the WC stability function for $\overline{\epsilon_k}$ and most for the APKE stability function. Because of the common factor u_* in both $\kappa z\overline{\epsilon_k} \,/\, u_*^3$ and $-z/L$, the observed dependence of $\kappa z\overline{\epsilon_k} \,/\, u_*^3$ on $-z/L$ in Figure 11b are partly impacted by self-correlation between u_*^{-2} in the abscissa and u_*^{-3} in the ordinate, which is demonstrated by the similar increase of $\kappa z\overline{\epsilon_k} \,/\, u_*^3$ with $-z/L$ using randomly generated u_* (the green line in Figure 11b). Because $\overline{V}$ and the corresponding u_* at a given height are linearly correlated under near neutral conditions (small $|z/L|$) (Sun et al., 2016), but not much under free convective conditions (large negative z/L) due to contribution of positive buoyancy to u_*, the increase of $\overline{\epsilon_k}$ with $-z/L$ could be less dramatic than its non-dimensionalized value with $-z/L$. We apply the observed u_* at 1.5 m under the most convective and the most windy conditions from CASES-99 into the WC and the APKE stability functions to estimate the corresponding values of $\overline{\epsilon_k}$ at 1.5 m. We find that with $u_* = 0.9$ m s^{-1} under the most neutral condition, $\overline{\epsilon_k}$ would be 1.3 and 0.7 W m^{-3} based on the WC and APKE $\overline{\epsilon_k}$ stability functions, respectively; with $u_* = 0.23$ m s^{-1} under the most convective condition, $\overline{\epsilon_k}$ would be 0.4 and 1.8 W m^{-3} for the two $\overline{\epsilon_k}$ stability functions. That is, $\overline{\epsilon_k}$ would increase with $-z/L$ based on the APKE stability function, but decrease with $-z/L$ based on the WC stability function. We use the APKE stability function here as it agrees with our spectrum analyses.

We then apply the high quality $\overline{\epsilon_k}$ measurement by Piper and Lundquist (2004) at the CASES-99 site to calibrate the magnitude of $\overline{\epsilon_k}$ on the convective day. Using a constant-temperature hot-wire anemometer at 3 m sampled at 9,600 samples per second, Piper and Lundquist (2004) calculated $\overline{\epsilon_k}$ under neutral conditions with the value of $\overline{V}$ similar to that on the most neutral condition during CASES-99 and found $\overline{\epsilon_k}$ being

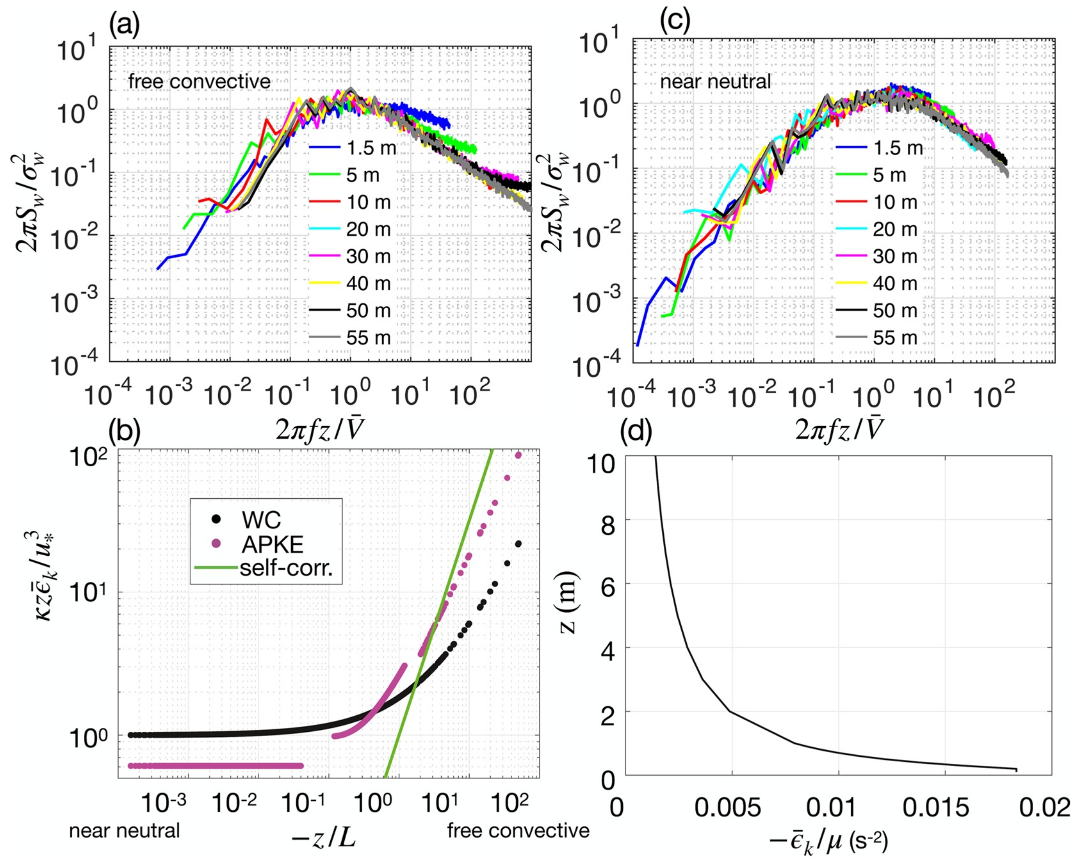

Figure 11. Normalized vertical velocity w power spectra $S_w(z)$, $2\pi fS_w(z)\ /\ \sigma_w^2(z)$, as functions of normalized frequency $2\pi fz\ /\ \bar{V}(z)$ at eight observation heights (a) under unstable conditions (from 1600 to 2000 UTC on 10 October) and (c) under near neutral conditions (from 0400 to 0800 UTC on 17 October), where $\sigma_w(z)$ is the standard deviation of w. (b) Relationships between the non-dimensionalized kinetic energy dissipation $\bar{\epsilon}_k$, $\kappa z\bar{\epsilon}_k\ /\ u_*^3$, and the stability parameter $-z/L$ from near neutral to free convective conditions by Wyngaard and Coté (1971) (WC) and Albertson et al. (1997) (APKE), where the self-correlation contribution of u_* to the relationship is marked as the green line. The measurements from the lowest sonic anemometer (1.5 or 0.5 m) were used to calculate $-z/L$. (d) The height dependence of $-\bar{\epsilon}_k\ /\ \mu$ in Equation 8 is estimated with the mean logarithmic wind $\bar{V}$ only using the most convective $u_* = 0.23$ m s^{-2} during CASES-99. Note that the increase of w turbulence intensity with decreasing height in (a) is consistent with the increase of the energy dissipation with decreasing height in (d).

about 1 Wm^{-3}. Assuming the APKE $\bar{\epsilon}_k$ stability function is valid, $\bar{\epsilon}_k$ at 3 m above the surface would be about 5 Wm^{-3} around noon on the convective day.

We then estimate the magnitude of the vertically integrated $\bar{\epsilon}_k$, Q_{DK} on the convective day. Based on the analytic formula for $\bar{\epsilon}_k$ in Equation 8, and assuming $\bar{\epsilon}_k$ is contributed mainly by the mean wind described by the log-linear profile with the observed $z_o = 0.05$ m at the site (Sun, 2011), the surface $\bar{\epsilon}_k$ would be about 6 times larger than the one at 3 m because the dependence of $\bar{\epsilon}_k$ on the second vertical derivative of wind speed. Using the averaged $\bar{\epsilon}_k$ between 3 m and the surface to represent the mean $\bar{\epsilon}_k$ in the AL, Q_{DK} would be $Q_{DK} = \int_0^{5\,m} \bar{\epsilon}_k dz \approx (5 + 5 \times 6)\ /\ 2 \times 5 \approx 88$ Wm^{-2}.

Based on our analyses of all the terms in Equation 19, only Q_{MA}, Q_{MS}, and Q_{DK} have the similar diurnal variation as Q_{res} has; Q_{DK} is estimated to have the largest magnitude among these three terms, which has the similar order of the magnitude as Q_{res} does. Thus, the energy consumption of Q_{DK} could potentially explain where the missing energy of Q_{res} goes to. Contribution of energy dissipation to the SEI was also found important by Li and Wang (2020).

5.2.2.3. Hypothesis for the Surface Energy Imbalance

Based on the above analyses, the thermal energy transfer across the surface Q_C is likely to be diverted near the surface under free convective conditions. The energy transfer for enhancing TKE prevents the molecular heat transfer across the surface from being completely transferred to Q_H at z. Free convective conditions require positive buoyancy to persist, that is, the non-hydrostatic energy transfer due to the negative density flux is always present in the AL and contributes to the kinetic energy increase. Because of air viscosity, the TKE increase would lead to TKE dissipation in the process of the energy cascade and to consequent dissipation heating. Besides TKE changes through kinetic energy transfer and mechanical generation of TKE through shear, the thermal energy consumption for the non-hydrostatic energy transfer leads to extra TKE increase, extra TKE dissipation and extra dissipation heating within the AL. Under free convective conditions when the mechanical generation of TKE is negligible, that is, both wind speed near the surface and the vertical variation of wind are weak, the energy for TKE increase and its corresponding energy dissipation is from the molecular heat transfer across the surface. This energy transfer path is not included in the traditional thermal energy balance. In addition, the increase of $\overline{\epsilon_k}$ toward the surface would lead to the increase of the dissipation heating $\overline{\epsilon_t}$ toward the surface, which implicitly contributes to the increasing air warming toward the surface. That is, the observed strong air temperature decrease with height around noon (~6 K decrease between the surface and 1 m in Figure 7a) when the maximum TKE occurs on the convective day could be partially contributed by the increased heating from $\overline{\epsilon_t}$ toward the surface. Although dissipation heating $\overline{\epsilon_t}$ results from the physical process that reduces the upward thermal energy transfer and does not contribute to the SEI directly (Equation 18), further increasing thermal energy near the surface besides the direct heat transfer from the molecular diffusion across the surface would strengthen positive buoyancy and non-hydrostatic energy transfer. Consequently, Q_H measured at the top of the AL would be less than Q_C, resulting in the SEI based on the traditional formulation for the SEI. In contrast, mechanically generated turbulence eddies from wind shear draw energy from the mechanical forcing from horizontal pressure gradients. Thus, mechanically generated turbulent mixing would transfer the surface heat upward effectively between z and the surface especially under strong winds regardless whether the surface is being heated or cooled. Based on total energy conservation, we could possibly examine the energy transfers between thermal and kinetic energy changes and understand different energy transfers under convective and windy conditions.

6. Summary

Fundamentally, investigation of the so-called SEB is to apply measurements pertinent to the thermal energy balance in both soil and air layers that are connected through molecular heat and moisture transfer across the ground surface. As we cannot directly measure the molecular heat and moisture transfer across the interface easily, the SEB can be investigated by combining the thermal energy balance in the soil and air layers with cancellation of the same molecular heat and moisture transfer at the surface. Thus, the investigation of the SEB becomes the study of the thermal energy balance in both the soil and the air layers with measurements of all the energy transfers except the molecular heat and moisture transfer. The observed systematic surface energy imbalance over a variety of surfaces has puzzled the community for a long time. Guided by the concept of total energy conservation, we re-examine the surface energy imbalance using the CASES-99 field measurements and propose a new hypothesis for explaining the diurnally varying systematic bias of the imbalance.

Consistent with the observed imbalance in the literature, we have identified that the surface energy imbalance is uniquely related to air-land surface temperature differences with large positive values under free convective conditions, small negative values under stable conditions, and approximately zero under neutral conditions. Physically, any air-surface temperature difference would contribute to a thermal energy transfer across the surface. Due to the relatively slow and ineffective molecular heat and moisture transfer across the surface, warm or cold and moist air from the surface accumulates near the surface until turbulence eddies transfer it away from the surface. Using high-vertical-resolution and fast response thermocouple measurements of air temperature, we find that heat fluxes indeed increase toward the surface under free convective conditions. The observed dependence of the surface energy imbalance on atmospheric stratification indicates that thermally generated turbulence eddies under free convective conditions when wind speed is weak are ineffective in transferring heat and moisture away from the surface; whereas mechanically generated turbulence eddies under strong winds do. Thus, the study of the SEB becomes an investigation of how the thermal energy originated from the molecular heat diffusion is transferred in the atmospheric surface layer and why these energy transfer terms are systematically different among convective, stable, and near neutral conditions.

Applying the thermal energy balance derived based on total energy conservation to the air and the soil layers joint at the surface, we have identified three energy transfer terms that are not considered in the traditionally formulated SEB as shown in Equation 18. Two of them are related to the thermal energy change due to temperature variations of water mass flowing through an open system, one in the soil layer, and the other in the air layer. This special characteristic of an open system is traditionally overlooked in investigation of the SEB. Not counting these energy transfer terms would contribute to the observed imbalance. Using the CASES-99 observations, the two terms are estimated to be relatively small in comparison with the observed imbalance. The third missing term is the non-hydrostatic energy transfer that is not described in the traditional thermal energy balance and is alluded by Sun (2019) and further illustrated in Appendix A based on the concept of total energy conservation.

Fundamentally, the thermal energy balance should be derived based on total energy conservation. Due to molecular heat transfer across the surface and air density changes from thermal expansion/contraction, vertical density fluxes are generated by either positive buoyancy or wind shear, leading to potential energy changes, hydrostatic imbalance, and non-hydrostatic energy transfer. This non-hydrostatic energy transfer is included in the kinetic energy balance, but not in the traditional thermal energy balance based on the first law of thermodynamics that excludes kinetic energy. Based on the concept of total energy conservation, available energy for thermal energy changes has to be adjusted by the amount of the non-hydrostatic energy transfer used for changing kinetic energy. This non-hydrostatic energy transfer changes signs between convective and stable conditions due to negative air density fluxes from positive buoyancy and positive air density fluxes from wind shear in the stable atmospheric surface layer. The diurnal variation of the non-hydrostatic energy transfer estimated using the CASES-99 data set is consistent with the observed diurnal variation of the imbalance.

We then estimate the magnitude of the non-hydrostatic energy transfer through its relationship to the energy transfer in the kinetic energy balance because CASES-99 was not designed for direct estimation of the magnitude of the non-hydrostatic energy transfer especially not for the rapid vertical variation of energy transfers near the surface. We find that the temporal variation of the non-hydrostatic energy transfer on the most convective day during CASES-99 matches the temporal variations of TKE, which is directly related to TKE dissipation as suggested in Equation 13. The magnitude of TKE dissipation integrated over the bottom 5-m atmospheric layer is then estimated by examining vertical variations of vertical velocity spectra with the atmospheric instability, the analytic formulation of the TKE dissipation with wind speed variation, and the observed magnitude and instability dependence of TKE dissipation in the literature. We find that as a result of the enhanced kinetic energy from the non-hydrostatic energy transfer under the most convective condition during CASES-99, the vertically integrated TKE dissipation within the surface layer could be comparable with the magnitude of the observed imbalance and the largest energy consumption for the imbalance derived in Equation 19. The seemingly large vertically integrated energy dissipation near the surface under free convective conditions is related to the exponential increase of the energy dissipation toward the surface and the observed increase of the energy dissipation with increasing unstable atmosphere stratification. The dissipation heating as the by-product of the energy dissipation contributes to heating the air layer, not directly to the imbalance.

Investigation of energy transfer in this study suggests that the ineffective heat and moisture transfer by convective eddies could be due to the non-hydrostatic energy transfer and the resulting thermal energy consumption for energy dissipation near the surface in reducing the available energy for turbulent energy transfer. That is, part of the thermal energy from molecular diffusion is diverted near the surface, and the turbulent heat transfer observed at a distance above the surface does not reflect the surface heat transfer by molecular diffusion even with inclusion of the heat storage associated with the air warming in the surface layer. In contrast, mechanically generated turbulence eddies by wind shear consume energy generated by mechanical pressure work and can effectively transport heat and moisture upward especially when wind shear is strong. Consequently, vertical air density fluxes and the corresponding non-hydrostatic energy transfer are near zero even surface heating/cooling may be present, and the surface energy is approximately balanced based on the traditional thermal energy balance formulation.

Currently all numerical models are based on the traditional thermal energy balance, in which the energy consumption for generating the non-hydrostatic energy transfer from diabatic heating is not considered while the impact of this non-hydrostatic energy transfer, at least part of it, on changing kinetic energy is. In addition, commonly used parameterizations of the surface heat transfer by using the temperature difference between the air temperature at a given height and the surface radiation temperature are essentially to equate the fast turbulent heat transfer across a relatively large spatial scale with the slow molecular diffusion across a relatively small spatial scale (Udina et al., 2016). The physical processes for explaining the surface energy imbalance presented here may provide new insights on air-land parameterization for heat and water vapor transfer as well as the constraint of total energy conservation on the atmospheric thermodynamics. The SEB impacted by surface heterogeneity and non-stationarity present challenges and requires further investigations guided by total energy conservation. Adequate measurements for quantifying thermal energy transfer to identify missed energy transfer in the traditional thermal energy balance is needed for understanding not only the surface energy imbalance but also fundamental thermodynamics and energy conservation in the atmosphere.

Appendix A: A Brief Review of the Derivation of the Thermal Energy Balance

The detailed physical explanation, derivation, and observational evidence for the new thermal energy balance can be found in Sun (2019). Further explanation and clarification of the derivation are given here. As described in Sun (2019) and Section 2 in this study, the first law of thermodynamics in many engineering text books is regarding all the energy of a system as a result of the work done by the system and the net heat transfer, thus, it is also called total energy conservation. The first law of thermodynamics commonly used by geophysicists is only valid when the fluid is at rest; that is, the kinetic energy related to observable air motions is zero, which is a special situation of total energy conservation. Mathematically, total energy conservation for a system can be expressed as

$$\rho_a \frac{dE_t}{dt} = \rho_a \frac{dE_k}{dt} + \rho_a \frac{dE_i}{dt} + \rho_a \frac{dE_p}{dt} = Q + F_m, \tag{A1}$$

where ρ_a is the air density, E_t, E_k, E_i, and E_p are specific total energy, kinetic energy, internal energy, and potential energy of the system, Q is the net heating to the system, and $F_m = -\nabla \cdot (\vec{V}p) + \epsilon$ is the mechanical forcing to the system ($\vec{V}$ is the wind vector, p is the air pressure, and ϵ is the viscous stress related to the rate of angular deformation done to the system).

As Bird et al. (2007) clearly stated that there is no conservation law for internal energy, the internal energy balance has to be derived based on total energy conservation with kinetic energy conservation. Kinetic energy conservation is commonly derived from momentum conservation. For geophysical applications, the mechanical force includes gravity force. That is, kinetic energy conservation can be expressed in two dimensions for simplicity as

$$\rho_a \frac{dE_k}{dt} = -\rho_a \frac{dE_p}{dt} - \vec{V} \cdot \nabla p + \epsilon_k = -w\left(\frac{\partial p}{\partial z} + \rho_a g\right) - u\frac{\partial p}{\partial x} + \epsilon_k \equiv q_{NH} - u\frac{\partial p}{\partial x} + \epsilon_k, \tag{A2}$$

where $\vec{V} = (u\vec{i}, w\vec{k})$ ($\vec{i}$ and $\vec{k}$ are unit vectors in horizontal and vertical directions), ϵ_k is the rate of dissipation of mechanical energy due to viscosity, $q_{NH} \equiv -w(\partial p/\partial z + \rho_a g)$, and potential energy changes, $\rho_a dE_p/dt = \rho_a wg$ is applied.

Because of the inclusion of potential energy changes in kinetic energy conservation derived from momentum conservation, using Equation A2 for kinetic energy changes in total energy conservation Equation A1, the total energy balance would be expressed as

$$\rho_a \frac{dE_k}{dt} + \rho_a \frac{dE_i}{dt} = Q + F_m, \tag{A3}$$

Thus, the internal/thermal energy balance is

$$\rho_a \frac{dE_i}{dt} = -\rho_a \frac{dE_k}{dt} + Q + F_m. \tag{A4}$$

Substituting the kinetic energy balance, Equation A2 into Equation A4 following the standard derivation in all the textbooks in the atmospheric dynamics with the usage of potential temperature, the thermal energy balance with q_{NH} would emerge. Decomposing the thermal energy balance into mean and perturbed states with the Reynolds decomposition, one would have Equation 10.

In the atmosphere, potential energy can be balanced by pressure forcing, that is, vertical variations of the atmospheric pressure, as the hydrostatic balance. Once the balance is perturbed by vertical air density fluxes under the forcing of either Q, or F_m, or both, such as by positive buoyancy or wind shear when the atmosphere is stably stratified, the hydrostatic imbalance would trigger the non-hydrostatic energy transfer, $\overline{q}_{NH}$ (Equation 9), leading to a new stage of hydrostatic balance. The non-hydrostatic energy transfer, $\overline{q}_{NH}$, would result in kinetic energy changes as evident in observed thermal plumes. The non-hydrostatic energy transfer $\overline{q}_{NH}$ (Equation 9) is the familiar term in the turbulent kinetic energy balance, for example, Equation 2.72 in Garratt (1992), except most studies only concentrate on the first component in $\overline{q}_{NH}$, that is, the heat flux transfer.

Physically, the new thermal energy balance, Equation 10, means that as a result of the energy consumption for changing kinetic energy through $\overline{q}_{NH}$ out of the energy source $Q + F_m$ for the system, the internal energy change, $\rho_a dE_i/dt$ would be negatively impacted by this energy transfer. A positive $\overline{q}_{NH}$ for increasing kinetic energy in Equation A2 would have a negative $\overline{q}_{NH}$ for changing thermal energy. In other words, more energy used for increasing $\rho_a dE_k/dt$ would result in less increase in $\rho_a dE_i/dt$ for a given energy input $Q + F_m$ and vice versa. The impact of $Q + F_m$ on kinetic energy changes is considered in the turbulent atmosphere but the consequence of kinetic energy changes on thermal energy changes is not included in the traditional thermal energy balance derived from the first law of thermodynamics where air motion is assumed to be negligibly small.

Bird et al. (2007) in their well known text book mainly for engineering used the mechanical energy balance for an isothermal fluid system (their Equations 7.4–2) in deriving the internal energy balance (their Equations 15.2–6). Thus, the kinetic energy balance in Bird et al. (2007) is only influenced by mechanical forcing, F_m, and could not be impacted by net heating Q. As a result, the internal energy balance is not influenced by kinetic energy changes in their derivation.

Appendix B: Derivation of the Thermal Energy Balance in the Air and the Soil Layers

We vertically integrate the new thermal energy balance for the moist air in the AL, Equation 10, from the surface to z, which consists of the thin MDL below $z = \delta z_a$ and the TSL between δz_a and z as

$$\begin{aligned}
&\int_0^z \overline{\rho}_a[c_{pd}(1-\overline{q}) + c_{pv}\overline{q}]\frac{\partial\overline{\theta}}{\partial t}dz + \int_0^{\delta z_a} k_T \frac{\partial^2\overline{\theta}}{\partial z^2}dz + \int_{\delta z_a}^z \overline{\rho}_a[c_{pd}(1-\overline{q}) + c_{pv}\overline{q}]\frac{\partial\overline{w'\theta'}}{\partial z}dz \\
&= -\int_0^z \frac{\partial Q_{RA}}{\partial z}dz - (c_{pv} - c_{pd})\left(\int_0^{\delta z_a} k_q \frac{\partial\overline{q}}{\partial z}\frac{\partial\overline{\theta}}{\partial z}dz + \int_{\delta z_a}^z \overline{\rho}_a\overline{w'q'}\frac{\partial\overline{\theta}}{\partial z}dz\right) \\
&+\int_0^z \overline{\epsilon}_t dz - \int_0^z \overline{q}_{NH}dz,
\end{aligned} \tag{B1}$$

where ρ_a in kg m^{-3} is the air density, q in kg kg^{-1} is the air specific humidity, c_{pd} and c_{pv} in W s K^{-1} kg^{-1} are the heat capacities for dry air and water vapor at constant pressure, θ in K is potential temperature, t in s is time, z in m is the turbulence observation height, k_T in WK^{-1} m^{-1} and k_q in kg m^{-1} s^{-1} are the air thermal conductivity and the diffusion coefficient for water vapor, Q_{RA} in Wm^{-2} is the vertically integrated radiative heating/cooling, $\overline{w'\theta'}$ in ms^{-1}K and $\overline{w'q'}$ in ms^{-1} kg kg^{-1} are the kinetic heat flux and the water vapor flux in the AL, $\overline{\epsilon_t}$ in W m^{-3} is the dissipation heating, and q_{NH} in Wm^{-3} is the non-hydrostatic energy transfer. In Equation B1, $[c_{pd}(1-\overline{q}) + c_{pv}\overline{q}]$ represents c_p in Equation 10.

In this study, we consider $q < 20$ g Kg^{-1}, thus $\theta_v \approx \theta$ and $\overline{w'\theta_v'} \approx \overline{w'\theta'}$. Equation B1 can be expressed as

$$\Delta Q_a + Q_H - Q_C = Q_{RA} - Q_{MA} + Q_{DT} - Q_{NH}, \tag{B2}$$

where

$$\Delta Q_a = \int_0^z \overline{\rho}_a[c_{pd}(1-\overline{q}) + c_{pv}\overline{q}]\frac{\partial\overline{\theta}}{\partial t}dz, \tag{B3}$$

$$Q_H = \overline{\rho}_a c_{pd}(\overline{w'\theta'})_z, \tag{B4}$$

$$Q_C = -k_T\left(\frac{\partial\overline{\theta}}{\partial z}\right)_0 = -k_T(T_{a0} - T_{s0}), \tag{B5}$$

$$Q_{RA} = -\int_0^z \frac{\partial Q_{RA}}{\partial z}dz = [(L_\uparrow - L_\downarrow)_0 - (L_\uparrow - L_\downarrow)_z + (S_\uparrow - S_\downarrow)_0 - (S_\uparrow - S_\downarrow)_z], \tag{B6}$$

$$Q_{MA} = (c_{pv} - c_{pd})\left(\int_0^{\delta z_a} k_q \frac{\partial\overline{q}}{\partial z}\frac{\partial\overline{\theta}}{\partial z}dz + \int_{\delta z_a}^z \overline{\rho}_a \overline{w'q'}\frac{\partial\overline{\theta}}{\partial z}dz\right), \tag{B7}$$

$$Q_{DT} = \int_0^z \overline{\epsilon_t}dz, \tag{B8}$$

$$Q_{NH} = \int_0^z \overline{q}_{NH}dz. \tag{B9}$$

The subscript represents the height where the variable is measured; for example, $(\overline{w'\theta'})_z$ in Equation B4 represents $(\overline{w'\theta'})$ at height z. In Equation B5, T_{a0} and T_{s0} represent the air and the soil temperature at the surface. In Equation B6, $S_\downarrow$, $S_\uparrow$, $L_\downarrow$, and $L_\uparrow$ are the downward and upward short and longwave irradiance, respectively. At $z = \delta z_a$ where the MDL transitions to the TSL, molecular diffusion is replaced by turbulent transfer, such as

$$-k_T\left(\frac{\partial\overline{\theta}}{\partial z}\right)_{\delta z_a} \approx \overline{\rho}_a c_{pd}\left(\overline{w'\theta'}\right)_{\delta z_a}, \tag{B10}$$

$$-k_q\left(\frac{\partial\overline{q}}{\partial z}\right)_{\delta z_a} \approx \overline{\rho}_a\left(\overline{w'q'}\right)_{\delta z_a}. \tag{B11}$$

Because of the negligibly small air flow in the SL, $q_{NH} \approx 0$, the traditional thermal energy balance is valid in the SL. Thus, the thermal energy balance in the SL in W m^{-3} can be expressed by following De Vries (1958) and Milly and Eagleson (1980) as

$$C\frac{\partial T_s}{\partial t} + \lambda_*\frac{\partial^2 T_s}{\partial z^2} + \rho_l c_{pl} F_l \frac{\partial T_s}{\partial z} = -\frac{\partial Q_{RS}}{\partial z} + L_0\frac{\partial E}{\partial z}. \tag{B12}$$

10.1029/2020JD034219

Equation B12 describes the thermal energy change in the soil layer that consists of dry soil, air, water vapor and liquid water at the LHS balances the thermal forcing of the vertical radiative divergence, $\partial Q_{RS}/\partial z$, and the latent heat release, $L_0 \partial E/\partial z$ (L_0 in W s Kg^{-1} and E in Kg m^{-2} s^{-1} are the latent heat of vapourization and water vapor fluxes, respectively), in the soil layer at the RHS. The terms from the left to the right on the LHS of Equation B12 represent the temporal change of the thermal energy, the thermal conduction, and the vertical thermal energy transfer by liquid water.

In deriving Equation B12, we assume that the following terms in Equation B12 are negligibly small: (a) thermal energy transfer associated with the air flow in the soil layer in comparison with liquid and soil thermal energy changes, (b) energy for air expansion in the SL, (c) heating associated with TKE dissipation, (d) the Defour effect resulted from temperature changes associated with diffusion from different types of particles, (e) internal heat sources such as the heat released during decay of radioactive soil minerals or the microbial decomposition of soil organic matter, and (f) differential heat of soil wetting. Because of assumption (a), pressure pumping effects on heat transfer are ignored (e.g., Clarke et al., 1987; Takle et al., 2004).

In Equation B12, T_s in K is the soil temperature. The heat coefficient C can be expressed as $C = c_s\rho_s(1 - \theta_d - \theta_v - \theta_l) + c_{pd}\rho_d\theta_d + c_{pv}\rho_v\theta_v + c_{pl}\rho_l\theta_l \approx c_s\rho_s(1 - \theta_l) + c_{pl}\rho_l\theta_l$, where c_s, c_{pd}, c_{pv}, and c_{pl} in W s K^{-1} kg^{-1} are the specific heat for dry soil, air, water vapor, and liquid water at a constant pressure, ρ_s, ρ_d, ρ_v, and ρ_l in kg m^{-3} are the dry soil, dry air, water vapor and liquid water densities, and θ_d, θ_v, and θ_l in m^3 m^{-3} are volumes of dry air, water vapor, and liquid water per bulk volume (the sum of soil, dry air, water vapor, and liquid water volumes). The approximation for C is due to the fact that $c_s\rho_s$ and $c_{pl}\rho_l$ are much larger than $c_{pd}\rho_d$ and $c_{pv}\rho_v$ ($c_s \approx 800$ W s K^{-1} kg^{-1}, $c_{pl} = 4128$ W s K^{-1} kg^{-1}, $c_{pd} = 1004$ W s K^{-1} kg^{-1}, $c_{pv} = 1952$ W s K^{-1} kg^{-1}, $\rho_d \approx 1.2$ kg m^{-3}, $\rho_v \approx 0.1$ kg m^{-3}, $\rho_l = 1{,}000$ kg m^{-3}, and $\rho_s \approx 840$ kg m^{-3}) (Kreith & Goswami, 2004; Norton, 2005). The coefficient λ_* in WK^{-1} m^{-1} is the apparent thermal conductivity of soil including effects of diffusive transport of water vapor. The term $F_l = w_l\theta_l$ in m s^{-1} (w_l represents the vertical motion of liquid water) represents the vertical liquid water flux due to infiltration or capillary water flow toward the surface and varies with soil moisture as well as soil temperature. Because c_{pl} is more than twice of c_{pv} and about four times c_{pd}, we only focus on the heat transfer from the vertical liquid water flux in the last term on the LHS of Equation B12.

Vertically integrating Equation B12 from $z = -\delta z_s$ to $z = 0$, we have

$$\Delta Q_s + Q_G = R_{net} - Q_C - Q_E - Q_{MS}, \tag{B13}$$

where

$$\Delta Q_s = \int_{-\delta z_s}^{0} C \frac{\partial T_s}{\partial t} dz, \tag{B14}$$

$$R_{net} = -\int_{-\delta z_s}^{0} \frac{\partial Q_{RS}}{\partial z} dz \approx -(Q_{RS})_0 = (L_\downarrow - L_\uparrow)_0 + (S_\downarrow - S_\uparrow)_0, \tag{B15}$$

$$Q_G = \lambda_* \left(\frac{\partial T_s}{\partial z}\right)_{-\delta z_s}, \tag{B16}$$

$$Q_{MS} = \int_{-\delta z_s}^{0} \rho_l c_{pl} F_l \frac{\partial T_s}{\partial z} dz, \tag{B17}$$

$$Q_E = L_0 \int_{-\delta z_s}^{0} \frac{\partial E}{\partial z} dz = L_0 E. \tag{B18}$$

Because the thermal energy transfer out of the SL at $z = 0$, Q_C, matches the thermal energy transfer into the AL at $z = 0$, Q_C in Equation B13 is the same as the Q_C in Equation B5. Applying liquid water mass conservation, we have

$$\frac{\partial \theta_l}{\partial t} + \frac{\partial F_l}{\partial z} = -\frac{1}{\rho_l}\frac{\partial E}{\partial z}, \tag{B19}$$

where

$$E \approx \overline{\rho}_a \left[\int_0^z \frac{\partial \overline{q}}{\partial t} dz + (\overline{w'q'})_z \right]. \quad \text{(B20)}$$

Data Availability Statement

The observational data used in the study are available from the cited reference for the field campaign, CASES-99 (UCAR/NCAR-Earth Observing Laboratory, 2016).

Acknowledgments
We would like to acknowledge the field support from the Earth Observing Laboratory of the National Center for Atmospheric Research (NCAR). We would also like to thank Peggy LeMone, Donald Lenschow, and Steve Oncley at NCAR for stimulating discussions on the SEB, Anthony C. Delany for collecting the soil calibration data, Xuhui Lee for providing the work of Bird et al. (2007) and valuable comments, Dr. Thomas Foken for his constructive comments, an anonymous review for providing important viscous work relevant to the SEB and helpful comments, and Terry Murray for her great efforts for tracking historical SEB investigations.
RMB was supported by the NOAA/CSL Air Quality Program, the Atmospheric Science for Renewable Energy (ASRE) Program, and in part by the NOAA Cooperative Agreement with CIRES, NA17OAR4320101.
JS started this work when she worked at NCAR, which is managed by the University Corporation for Atmospheric Research under sponsorship by the National Science Foundation (NSF). JS is currently a program director of the Physical and Dynamic Meteorology program at NSF. This work was completed under the Independent Research & Development (IR&D) program at NSF. The views expressed here do not represent the official position of the U.S. Government. Any opinions, findings and conclusions, or recommendations expressed in this publication are those of the authors.

References

Albertson, J. D., Parlange, M. B., Kiely, G., & Eichinger, W. E. (1997). The average dissipation rate of turbulent kinetic energy in the neutral and unstable atmospheric surface layer. *Journal of Geophysical Research*, *102*(D12), 13423–13432. https://doi.org/10.1029/96jd03346

Albrecht, F. (1937). Die meßgeräte des wämeumsatzes der pflanzen-bestandenen erdorberfläche unter besonderer beücksichtigung von messungen in walde. *Zeitschrift für Angewandte Meteorologie*, *54*, 105–115.

Albrecht, F. (1940). *Untersuchungen über den wärmehaushalt der erdoberfläche in verschiedenen klimagebieten*. Springer-Verlag Berlin Heidelberg GmbH. https://doi.org/10.1007/978-3-662-42530-5

Aubinet, M., Grelle, A., Ibrom, A., Rannik, Ü., Moncrieff, J., Foken, T., et al. (1999). Estimates of the annual net carbon and water exchange of forests: The EUROFLUX methodology. *Advances in Ecological Research*, *30*, 113–175. https://doi.org/10.1016/S0065-2504(08)60018-5

Aubinet, M., Heinesch, B., & Yernaux, M. (2003). Horizontal and vertical Co_2 advection in a sloping forest. *Boundary-Layer Meteorology*, *108*, 397–417. https://doi.org/10.1023/a:1024168428135

Barr, A. G., Morgenstern, K., Black, T. A., McCaughey, J. H., & Nesic, Z. (2006). Surface energy balance closure by the eddy-covariance method above three boreal forest stands and implications for the measurement of the CO_2 flux. *Agricultural and Forest Meteorology*, *140*(1), 322–337. https://doi.org/10.1016/j.agrformet.2006.08.007

Batchelor, G. K. (1967). *An introduction to fluid dynamics*. Cambridge University Press.

Bennett, C. O., & Myers, J. E. (1962). *Momentum, heat, and mass transfer*. McGraw-Hill.

Bird, R. B., Stewart, W. E., & Lightfoot, E. N. (2007). Transport phenomena, revised (Vol. 12). J. Wiley & Son.

Bredehoeft, J. D., & Papaopulos, I. S. (1965). Rates of vertical groundwater movement estimated from the Earth's thermal profile. *Water Resources Research*, *1*(2), 325–328. https://doi.org/10.1029/wr001i002p00325

Brötz, B., Eigenmann, R., Dörnbrack, A., Foken, T., & Wirth, V. (2014). Early-morning flow transition in a valley in low-mountain terrain under clear-sky conditions. *Boundary-Layer Meteorology*, *152*(1), 45–63. https://doi.org/10.1007/s10546-014-9921-7

Burns, S. P., Blanken, P. D., Turnipseed, A. A., Hu, J., & Monson, R. K. (2015). The influence of warm-season precipitation on the diel cycle of the surface energy balance and carbon dioxide at a Colorado subalpine forest site. *Biogeosciences*, *12*(23), 7349–7377. https://doi.org/10.5194/bg-12-7349-2015

Burns, S. P., Frank, J. M., Massman, W. J., Patton, E. G., & Blanken, P. D. (2021). The effect of static pressure-wind covariance on vertical carbon dioxide exchange at a windy subalpine forest site. *Agricultural and Forest Meteorology*, *306*. https://doi.org/10.1016/j.agrformet.2021.108402

Burns, S. P., Horst, T. W., Jacobsen, L., Blanken, P. D., & Monson, R. K. (2012). Using sonic anemometer temperature to measure sensible heat flux in strong winds. *Atmospheric Measurement Techniques*, *5*, 2095–2111. https://doi.org/10.5194/amt-5-2095-2012

Burns, S. P., & Sun, J. (2000). Thermocouple temperature measurements from the CASES-99 main tower. In *14th Symposium on Boundary Layer and Turbulence* (pp. 285–288). American Meteorological Society.

Burns, S. P., Sun, J., Delany, A. C., Semmer, S. R., Oncley, S. P., & Horst, T. W. (2003). A field intercomparison technique to improve the relative accuracy of longwave radiation measurements and an evaluation of CASES-99 pyrgeometer data quality. *Journal of Atmospheric and Oceanic Technology*, *20*, 348–361. https://doi.org/10.1175/1520-0426(2003)020<0348:afitti>2.0.co;2

Charuchittipan, D., Babel, W., Mauder, M., Leps, J.-P., & Foken, T. (2014). Extension of the averaging time in eddy-covariance measurements and its effect on the energy balance closure. *Boundary-Layer Meteorology*, *152*(3), 303–327. https://doi.org/10.1007/s10546-014-9922-6

Charuchittipan, D., & Wilson, J. D. (2009). Turbulent kinetic energy dissipation in the surface layer. *Boundary-Layer Meteorology*, *132*(2), 193–204. https://doi.org/10.1007/s10546-009-9399-x

Clarke, G. K., Fisher, D. A., & Waddington, E. D. (1987). Wind pumping: A potentially significant heat source in ice sheets. In Proceedings of Symposium for the Physical Basis of Ice Sheet Modeling (Vol. 170, pp. 169–180).

Culf, A. D., Foken, T., & Gash, J. H. (2004). The energy balance closure problem. In *Vegetation, water, humans, and the climate: A new perspective on an interactive system*. Springer Science & Business Media.

Cuxart, J., Morales, G., Terradellas, E., & Yagüe, C. (2002). Study of coherent structures and estimation of the pressure transport terms for the nocturnal stable boundary layer. *Boundary-Layer Meteorology*, *105*, 305–328. https://doi.org/10.1023/a:1019974021434

De Groot, S. R., & Mazur, P. (2013). *Non-equilibrium thermodynamics*. Dover. (manufactured by Courier Corporation).

Delany, A. C., & Semmer, S. R. (1998). An integrated surface radiation measurement system. *Journal of Atmospheric and Oceanic Technology*, *15*(1), 46–53. https://doi.org/10.1175/1520-0426(1998)015<0046:aisrms>2.0.co;2

De Vries, D. A. (1958). Simultaneous transfer of heat and moisture in porous media. *Eos, Transactions American Geophysical Union*, *39*(5), 909–916. https://doi.org/10.1029/tr039i005p00909

Eder, F., De Roo, F., Kohnert, K., Desjardins, R. L., Schmid, H. P., & Mauder, M. (2014). Evaluation of two energy balance closure parametrizations. *Boundary-Layer Meteorology*, *151*(2), 195–219. https://doi.org/10.1007/s10546-013-9904-0

Eder, F., Schmidt, M., Damian, T., Träumner, K., & Mauder, M. (2015). Mesoscale eddies affect near-surface turbulent exchange: Evidence from lidar and tower measurements. *Journal of Applied Meteorology and Climatology*, *54*(1), 189–206. https://doi.org/10.1175/jamc-d-14-0140.1

Elagina, L. G., Zubkobskii, S. L., Kaprov, B. M., & Sokolov, D. Y. (1973). Experimental investigations of the energy balance near the surface (in Russian). *Trudy GGO*, *296*, 38–45.

Finnigan, J. J. (2004a). The footprint concept in complex terrain. *Agricultural and Forest Meteorology*, *127*(3), 117–129. https://doi.org/10.1016/j.agrformet.2004.07.008
Finnigan, J. J. (2004b). A re-evaluation of long-term flux measurement techniques part II: Coordinate systems. *Boundary-Layer Meteorology*, *113*(1), 1–41. https://doi.org/10.1023/b:boun.0000037348.64252.45
Finnigan, J. J., Clement, R., Malhi, Y., Leuning, R., & Cleugh, H. A. (2003). A re-evaluation of long-term flux measurement techniques part I: Averaging and coordinate rotation. *Boundary-Layer Meteorology*, *107*, 1–48. https://doi.org/10.1023/a:1021554900225
Foken, T. (1978). The molecular temperature boundary layer of the atmosphere over various surfaces. *Archiv für Meteorologie, Geophysik und Bioklimatologie, Serie A*, *27*(1), 59–67. https://doi.org/10.1007/bf02246461
Foken, T. (2008). The energy balance closure problem: An overview. *Ecological Applications*, *18*(6), 1351–1367. https://doi.org/10.1890/06-0922.1
Foken, T. (2017). *Micrometeorology* (2nd ed.), Springer Nature. https://doi.org/10.1007/978-3-642-25440-6
Foken, T., Aubinet, M., Finnigan, J. J., Leclerc, M. Y., Mauder, M., & Paw U, K. T. (2011). Results of a panel discussion about the energy balance closure correction for trace gases. *Bulletin of the American Meteorological Society*, *92*(4), ES13–ES18. https://doi.org/10.1175/2011bams3130.1
Foken, T., Mauder, M., Liebethal, C., Wimmer, F., Beyrich, F., Leps, J.-P., & Bange, J. (2010). Energy balance closure for the LITFASS-2003 experiment. *Theoretical and Applied Climatology*, *101*(1–2), 149–160. https://doi.org/10.1007/s00704-009-0216-8
Foken, T., & Oncley, S. (1995). Workshop on instrumental and methodical problems of land surface flux measurements. *Bulletin of the American Meteorological Society*, *76*, 1191–1224. https://doi.org/10.1175/1520-0477-76.7.1191
Frank, J. M., Massman, W. J., Swiatek, E., Zimmerman, H. A., & Ewers, B. E. (2016). All sonic anemometers need to correct for transducer and structural shadowing in their velocity measurements. *Journal of Atmospheric and Oceanic Technology*, *33*, 149–167. https://doi.org/10.1175/JTECH-D-15-0171.1
Franssen, H. J. H., Stöckli, R., Lehner, I., Rotenberg, E., & Seneviratne, S. I. (2010). Energy balance closure of eddy-covariance data: A multisite analysis for European FLUXNET stations. *Agricultural and Forest Meteorology*, *150*(12), 1553–1567. https://doi.org/10.1016/j.agrformet.2010.08.005
Gao, Z., Bian, L., Hu, Y., Wang, L., & Fan, J. (2007). Determination of soil temperature in an arid region. *Journal of Arid Environments*, *71*(2), 157–168. https://doi.org/10.1016/j.jaridenv.2007.03.012
Garratt, J. R. (1992). The atmospheric boundary layer. In *Cambridge atmospheric and space science series* (p. 316). Cambridge University Press.
Geiger, R. (1927). *The climate near the ground* (1st ed.). Vieweg. https://doi.org/10.1007/978-3-642-91594-9
Geiger, R., Aron, R. H., & Todhunter, P. (1995). *The climate near the ground* (5th ed.). Harvard University Press. https://doi.org/10.1007/978-3-322-86582-3
Haverd, V., Cuntz, M., Leuning, R., & Keith, H. (2007). Air and biomass heat storage fluxes in a forest canopy: Calculation within a soil vegetation atmosphere transfer model. *Agricultural and Forest Meteorology*, *147*(3–4), 125–139. https://doi.org/10.1016/j.agrformet.2007.07.006
Heitman, J. L., Xiao, X., Horton, R., & Sauer, T. (2008). Sensible heat measurements indicating depth and magnitude of subsurface soil water evaporation. *Water Resources Research*, *44*(4), W00D05. https://doi.org/10.1029/2008wr006961
Heusinkveld, B. G., Jacobs, A. F. G., Holtslag, A. A. M., & Berkowicz, S. M. (2004). Surface energy balance closure in an arid region: Role of soil heat flux. *Agricultural and Forest Meteorology*, *122*(1), 21–37. https://doi.org/10.1016/j.agrformet.2003.09.005
Hillel, D. (1980). *Fundamentals of soil physics*. Academic Press.
Hillel, D. (1998). *Environmental soil physics*. Academic Press.
Horst, T. W., & Lenschow, D. H. (2009). Attenuation of scalar fluxes measured with spatially-displaced sensors. *Boundary-Layer Meteorology*, *130*, 275–300. https://doi.org/10.1007/s10546-008-9348-0
Horst, T. W., Semmer, S. R., & Maclean, G. (2015). Correction of a non-orthogonal, three-component sonic anemometer for flow distortion by transducer shadowing. *Boundary-Layer Meteorology*, *155*, 371–395. https://doi.org/10.1007/s10546-015-0010-3
Huang, J., Lee, X., & Patton, E. G. (2008). A modeling study of flux imbalance and the influence of entrainment in the convective boundary layer. *Boundary-Layer Meteorology*, *127*(2), 273–292. https://doi.org/10.1007/s10546-007-9254-x
Hupfer, P., Foken, T., & Panin, G. (1975). Existence and structure of the laminar boundary layer of the atmosphere in the near-shore zone of the sea. *Zeitschrift für Meteorologie*, *25*, 94–102.
Jacobs, A. F., Heusinkveld, B. G., & Holtslag, A. A. (2008). Toward closing the surface energy budget of a mid-latitude grassland. *Boundary-Layer Meteorology*, *126*(1), 125–136.
Kaimal, J. C. (1978). Sonic anemometer measurement of atmospheric turbulence, *Proceedings of the dynamic flow conference 1978 on dynamic measurements in unsteady flows* (pp. 551–565). https://doi.org/10.1007/978-94-009-9565-9_29
Kanda, M., Inagaki, A., Letzel, M. O., Raasch, S., & Watanabe, T. (2004). LES study of the energy imbalance problem with eddy covariance fluxes. *Boundary-Layer Meteorology*, *110*(3), 381–404. https://doi.org/10.1023/b:boun.0000007225.45548.7a
Kidston, J., Brummer, C., Black, T. A., Morgenstern, K., Nesic, Z., McCaughey, J. H., & Barr, A. G. (2010). Energy balance closure using eddy covariance above two different land surfaces and implications for CO_2 flux measurements. *Boundary-Layer Meteorology*, *136*, 196–218. https://doi.org/10.1007/s10546-010-9507-y
Kreith, F., & Goswami, D. Y. (2004). *The CRC handbook of mechanical engineering* (2nd ed.). CRC Press.
Kuo, K. K. (2005). *Principles of combustion* (2nd ed.). John Wiley & Sons, Inc.
Kustas, W. P., & Daughtry, C. S. T. (1990). Estimation of the soil heat flux/net radiation ratio from spectral data. *Agricultural and Forest Meteorology*, *49*(3), 205–223. https://doi.org/10.1016/0168-1923(90)90033-3
Lenschow, D. H., Li, X. S., Zhu, C. J., & Stankov, B. B. (1988). The stably stratified boundary layer over the great plains. *Boundary-Layer Meteorology*, *42*, 95–121. https://doi.org/10.1007/bf00119877
Lenschow, D. H., & Sun, J. (2007). The spectral composition of fluxes and variances over land and sea out to the mesoscale. *Boundary-Layer Meteorology*, *125*, 63–84. https://doi.org/10.1007/s10546-007-9191-8
Leuning, R., Van Gorsel, E., Massman, W. J., & Isaac, P. R. (2012). Reflections on the surface energy imbalance problem. *Agricultural and Forest Meteorology*, *156*, 65–74. https://doi.org/10.1016/j.agrformet.2011.12.002
Li, P., & Wang, Z.-H. (2020). A nonequilibrium thermodynamic approach for surface energy balance closure. *Geophysical Research Letters*, *47*(3), e2019GL085835. https://doi.org/10.1029/2019gl085835
Liebethal, C., & Foken, T. (2007). Evaluation of six parameterization approaches for the ground heat flux. *Theoretical and Applied Climatology*, *88*(1–2), 43–56. https://doi.org/10.1007/s00704-005-0234-0

Liebethal, C., Huwe, B., & Foken, T. (2005). Sensitivity analysis for two ground heat flux calculation approaches. *Agricultural and Forest Meteorology*, *132*(3), 253–262. https://doi.org/10.1016/j.agrformet.2005.08.001

Lindroth, A., Mölder, M., & Lagergren, F. (2010). Heat storage in forest biomass improves energy balance closure. *Biogeosciences*, *7*(1), 301–313. https://doi.org/10.5194/bg-7-301-2010

Mahrt, L. (1998). Flux sampling errors for aircraft and towers. *Journal of Atmospheric and Oceanic Technology*, *15*, 416–429. https://doi.org/10.1175/1520-0426(1998)015<0416:fsefaa>2.0.co;2

Mahrt, L., Sun, J., Vickers, D., MacPherson, J. I., Pederson, J. R., & Desjardins, R. L. (1994). Observations of fluxes and inland breezes over a heterogeneous surface. *Journal of the Atmospheric Sciences*, *51*, 2484–2499. https://doi.org/10.1175/1520-0469(1994)051<2484:oofaib>2.0.co;2

Mahrt, L., Vickers, D., & Sun, J. (2001). Spatial variations of surface moisture flux from aircraft data. *Advances in Water Resources*, *24*(9), 1133–1141. https://doi.org/10.1016/s0309-1708(01)00045-8

Mauder, M., Desjardins, R. L., Pattey, E., & Worth, D. (2010). An attempt to close the daytime surface energy balance using spatially-averaged flux measurements. *Boundary-Layer Meteorology*, *136*, 175–191. https://doi.org/10.1007/s10546-010-9497-9

Mauder, M., & Foken, T. (2006). Impact of post-field data processing on eddy covariance flux estimates and energy balance closure. *Meteorologische Zeitschrift*, *15*, 597–609. https://doi.org/10.1127/0941-2948/2006/0167

Mauder, M., Foken, T., & Cuxart, J. (2020). Surface-energy-balance closure over land: A review. *Boundary-Layer Meteorology*, *177*, 395–426. https://doi.org/10.1007/s10546-020-00529-6

Mauder, M., Genzel, S., Fu, J., Kiese, R., Soltani, M., Steinbrecher, R., et al. (2018). Evaluation of energy balance closure adjustment methods by independent evapotranspiration estimates from lysimeters and hydrological simulations. *Hydrological Processes*, *32*(1), 39–50. https://doi.org/10.1002/hyp.11397

Mauder, M., Jegede, O., Okogbue, E., Wimmer, F., & Foken, T. (2007). Surface energy balance measurements at a tropical site in West Africa during the transition from dry to wet season. *Theoretical and Applied Climatology*, *89*(3–4), 171–183. https://doi.org/10.1007/s00704-006-0252-6

McBean, G. A., & Elliott, J. A. (1975). The vertical transports of kinetic energy by turbulence and pressure in the boundary layer. *Journal of the Atmospheric Sciences*, *32*, 753–766. https://doi.org/10.1175/1520-0469(1975)032<0753:tvtoke>2.0.co;2

Milly, P. C. D. (1982). Moisture and heat transport in hysteretic, inhomogeneous porous media: A matric head-based formulation and a numerical model. *Water Resources Research*, *18*(3), 489–498. https://doi.org/10.1029/wr018i003p00489

Milly, P. C. D., & Eagleson, P. S. (1980). *The coupled transport of water and heat in a vertical soil column under atmospheric excitation*. (Technical Report No. Report No. 258). Department of Civil Engineering, Massachusetts Institute of Technology.

Nakai, T., Iwata, H., Harazono, Y., & Ueyama, M. (2014). An inter-comparison between Gill and Campbell sonic anemometers. *Agricultural and Forest Meteorology*, *195–196*, 123–131. https://doi.org/10.1016/j.agrformet.2014.05.005

Nelli, N. R., Temimi, M., Fonseca, R. M., Weston, M. J., Thota, M. S., Valappil, V. K., et al. (2020). Micrometeorological measurements in an arid environment: Diurnal characteristics and surface energy balance closure. *Atmospheric Research*, *234*, 104745. https://doi.org/10.1016/j.atmosres.2019.104745

Norton, P. (2005). Appendices. In F. Kreith, & D. Y. Goswami (Eds.), *The CRC handbook of mechanical engineering (chap. Appendices)*. The CRC Press

Oke, T. R. (2002). *Boundary layer climates* (2nd ed.), Routledge. https://doi.org/10.4324/9780203407219

Oliphant, A. J., Grimmond, C. S. B., Zutter, H. N., Schmid, H. P., Su, H.-B., Scott, S. L., et al. (2004). Heat storage and energy balance fluxes for a temperate deciduous forest. *Agricultural and Forest Meteorology*, *126*(3), 185–201. https://doi.org/10.1016/j.agrformet.2004.07.003

Oncley, S. P., Foken, T., Vogt, R., Kohsiek, W., DeBruin, H. A. R., Bernhofer, C., et al. (2007). The energy balance experiment EBEX-2000. Part I: Overview and energy balance. *Boundary-Layer Meteorology*, *123*(1), 1–28. https://doi.org/10.1007/s10546-007-9161-1

Panin, G. N., & Bernhofer, C. (2008). Parametrization of turbulent fluxes over inhomogeneous landscapes. *Izvestiya - Atmospheric and Oceanic Physics*, *44*(6), 701–716. https://doi.org/10.1134/s0001433808060030

Philip, J. R. (1957). Evaporation, and moisture and heat fields in the soil. *Journal of Meteorology*, *14*(4), 354–366. https://doi.org/10.1175/1520-0469(1957)014<0354:eamahf>2.0.co;2

Piper, M., & Lundquist, J. K. (2004). Surface layer turbulence measurements during a frontal passage. *Journal of the Atmospheric Sciences*, *61*(14), 1768–1780. https://doi.org/10.1175/1520-0469(2004)061<1768:sltmda>2.0.co;2

Roo, F. D., & Mauder, M. (2018). The influence of idealized surface heterogeneity on virtual turbulent flux measurements. *Atmospheric Chemistry and Physics*, *18*(7), 5059–5074.

Sánchez, J. M., Caselles, V., & Rubio, E. M. (2010). Analysis of the energy balance closure over a fluxnet boreal forest in finland. *Hydrology and Earth System Sciences*, *14*(8), 1487–1497. https://doi.org/10.5194/hess-14-1487-2010

Shao, M., Horton, R., & Jaynes, D. B. (1998). Analytical solution for one-dimensional heat conduction-convection equation. *Soil Science Society of America Journal*, *62*(1), 123–128. https://doi.org/10.2136/sssaj1998.03615995006200010016x

Steinfeld, G., Letzel, M. O., Raasch, S., Kanda, M., & Inagaki, A. (2007). Spatial representativeness of single tower measurements and the imbalance problem with eddy-covariance fluxes: Results of a large-eddy simulation study. *Boundary-Layer Meteorology*, *123*, 77–98. https://doi.org/10.1007/s10546-006-9133-x

Stoy, P. C., Mauder, M., Foken, T., Marcolla, B., Boegh, E., Ibrom, A., et al. (2013). A data-driven analysis of energy balance closure across FLUXNET research sites: The role of landscape scale heterogeneity. *Agricultural and Forest Meteorology*, *171–172*, 137–152. https://doi.org/10.1016/j.agrformet.2012.11.004

Sun, J. (2011). Vertical variations of mixing lengths under neutral and stable conditions during CASES-99. *Journal of Applied Meteorology and Climatology*, *50*, 2030–2041. https://doi.org/10.1175/jamc-d-10-05006.1

Sun, J. (2019). Incorporating the work done by vertical density fluxes in both kinetic and thermal energy conservation equations to satisfy total energy conservation. *Journal of Applied Meteorology and Climatology*, *58*, 213–230. https://doi.org/10.1175/jamc-d-17-0350.1

Sun, J., Burns, S. P., Delany, A. C., Oncley, S. P., Horst, T. W., & Lenschow, D. H. (2003). Heat Balance in the nocturnal boundary layer during CASES-99. *Journal of Applied Meteorology*, *42*, 1649–1666. https://doi.org/10.1175/1520-0450(2003)042<1649:hbitnb>2.0.co;2

Sun, J., Burns, S. P., Delany, A. C., Oncley, S. P., Turnipseed, A. A., Stephens, B. B., et al. (2007). CO_2 transport over complex terrain. *Agricultural and Forest Meteorology*, *145*, 1–21. https://doi.org/10.1016/j.agrformet.2007.02.007

Sun, J., Burns, S. P., Lenschow, D. H., Banta, R., Newsom, R., Coulter, R., et al. (2002). Intermittent turbulence associated with a density current passage in the stable boundary layer. *Boundary-Layer Meteorology*, *105*, 199–219. https://doi.org/10.1023/a:1019969131774

Sun, J., Esbensen, S. K., & Mahrt, L. (1995). Estimation of surface heat flux. *Journal of the Atmospheric Sciences*, *52*(17), 3162–3171. https://doi.org/10.1175/1520-0469(1995)052<3162:eoshf>2.0.co;2

Sun, J., Howell, J. F., Esbensen, S. K., Mahrt, L., Greb, C. M., Grossman, R., & LeMone, M. A. (1996). Scale dependence of air-sea fluxes over the western equatorial pacific. *Journal of the Atmospheric Sciences*, *53*, 2997–3012. https://doi.org/10.1175/1520-0469(1996)053<2997:sdoasf>2.0.co;2

Sun, J., Lenschow, D. H., LeMone, M. A., & Mahrt, L. (2016). The role of large-coherent-eddy transport in the atmospheric surface layer based on CASES-99 observations. *Boundary-Layer Meteorology*, *160*(1), 83–111. https://doi.org/10.1007/s10546-016-0134-0

Sun, J., Lenschow, D. H., Mahrt, L., Crawford, T. L., Davis, K. J., Oncley, S. P., et al. (1997). Lake-induced atmospheric circulations during BOREAS. *Journal of Geophysical Research*, *102*(D24), 29155–29166. https://doi.org/10.1029/97jd01114

Sun, J., Lenschow, D. H., Mahrt, L., & Nappo, C. (2013). The relationships among wind, horizontal pressure gradient, and turbulent momentum transport during CASES-99. *Journal of the Atmospheric Sciences*, *70*, 3397–3414. https://doi.org/10.1175/jas-d-12-0233.1

Sun, J., & Mahrt, L. (1994). Spatial distribution of surface fluxes estimated from remotely sensed variables. *Journal of Applied Meteorology*, *33*(11), 1341–1353. https://doi.org/10.1175/1520-0450(1994)033<1341:sdosfe>2.0.co;2

Sun, J., Takle, E. S., & Acevedo, O. C. (2020). Understanding physical processes represented by the monin-obukhov bulk formula for momentum transfer. *Boundary-Layer Meteorology*, *177*, 69–95. https://doi.org/10.1007/s10546-020-00546-5

Suomi, V. E. (1957). Sonic anemometer. In H. H. Lettau, & B. Davidson (Eds.), Exploring the atmosphere's first mile (Vol. 1, pp. 256–266). Pergamon

Swinbank, W. C. (1951). The measurement of vertical transfer of heat and water vapor by eddies in the lower atmosphere. *Journal of Meteorology*, *8*(3), 135–145. https://doi.org/10.1175/1520-0469(1951)008<0135:tmovto>2.0.co;2

Takle, E. S., Massman, W. J., Brandle, J. R., Schmidt, R. A., Zhou, X., Litvina, I. V., et al. (2004). Influence of high-frequency ambient pressure pumping on carbon dioxide efflux from soil. *Agricultural and Forest Meteorology*, *124*(3), 193–206. https://doi.org/10.1016/j.agrformet.2004.01.014

Twine, T. E., Kustas, W. P., Norman, J. M., Cook, D. R., Houser, P. R., Meyers, T. P., et al. (2000). Correcting eddy-covariance flux underestimates over a grassland. *Agricultural and Forest Meteorology*, *103*, 279–300. https://doi.org/10.1016/s0168-1923(00)00123-4

UCAR/NCAR-Earth Observing Laboratory. (2016). *5 minute statistics of ISFF data during CASES-99. Version 1.0*. UCAR/NCAR-Earth Observing Laboratory. https://doi.org/10.5065/D6ZS2TWW

Udina, M., Sun, J., Kosović, B., & Soler, M. R. (2016). Exploring Vertical turbulence structure in neutrally and stably stratified flows using the weather research and forecasting-large-eddy simulation (WRF-LES) Model. *Boundary-Layer Meteorology*, *161*(2), 355–374. https://doi.org/10.1007/s10546-016-0171-8

Van Orstrand, C. (1934). Temperature gradients. In Problems of petroleum geology (Vol. 989, p. 1021). Am. Assoc. Petrol. Geol Tulsa.

Webb, E. K., Pearman, G. I., & Leuning, R. (1980). Correction of flux measurements for density effects due to heat and water vapor transfer. *Quarterly Journal of Royal Meteorological Society*, *106*(447), 85–100. https://doi.org/10.1002/qj.49710644707

Wilson, K., Goldstein, A., Falge, E., Aubinet, M., Baldocchi, D., Berbigier, P., et al. (2002). Energy balance closure at FLUXNET sites. *Agricultural and Forest Meteorology*, *113*(1), 223–243. https://doi.org/10.1016/s0168-1923(02)00109-0

Wyngaard, J. C., & Coté, O. R. (1971). The budgets of turbulent kinetic energy and temperature variance in the atmospheric surface layer. *Journal of the Atmospheric Sciences*, *28*, 190–201. https://doi.org/10.1175/1520-0469(1971)028<0190:tbotke>2.0.co;2

Yamanaka, T., & Yonetani, T. (1999). Dynamics of the evaporation zone in dry sandy soils. *Journal of Hydrology*, *217*(1), 135–148. https://doi.org/10.1016/s0022-1694(99)00021-9

Zhou, Y., Li, D., Liu, H., & Li, X. (2018). Diurnal variations of the flux imbalance over homogeneous and heterogeneous landscapes. *Boundary-Layer Meteorology*, *168*(3), 417–442. https://doi.org/10.1007/s10546-018-0358-2